9 Galaxies

Henry C. Ferguson, Lee Armus, L. Felipe Barrientos, James G. Bartlett, Michael R. Blanton, Kirk D. Borne, Carrie R. Bridge, Mark Dickinson, Harold Francke, Gaspar Galaz, Eric Gawiser, Kirk Gilmore, Jennifer M. Lotz, R. H. Lupton, Jeffrey A. Newman, Nelson D. Padilla, Brant E. Robertson, Rok Roškar, Adam Stanford, Risa H. Wechsler

9.1 Introduction

The past decade of research has given us confidence that it is possible to construct a self-consistent model of galaxy evolution and cosmology based on the paradigm that galaxies form hierarchically around peaks in the dark matter density distribution. Within this framework, astronomers have made great progress in understanding the large-scale clustering of galaxies, as biased tracers of the underlying dark matter. We have started to understand how baryonic gas within the dark matter halos cools and collapses to form stars, and how the energy from star formation can feed back into the surrounding gas and regulate subsequent star formation.

However, at a fundamental level we still lack a solid understanding of the basic physics of galaxy evolution. We do not know for certain that all galaxies form at peaks in the dark matter density distribution. There is considerable debate about cold versus hot accretion of gas onto dark matter halos, and even more debate about which feedback mechanisms regulate star formation (photo-ionization, supernova winds, AGN, massive stellar feedback, etc.). We are reasonably certain that various feedback processes depend on environment, being different in rich clusters than in the low-density field, but the mechanisms are not understood. Some environmental and feedback effects (e.g., photo-ionization) can have an influence over long distances, which can in principle affect how stars connected to dark matter halos in different environments. We have a long way to go before declaring victory in our understanding of galaxy formation.

The galaxy evolution process is stochastic. The hierarchical paradigm tells us *statistically* when dark matter peaks of various masses and overdensities collapse and virialize. It tells us the statistical distribution of dark matter halo angular momenta, and it tells us statistically how dark matter halos grow via successive mergers and accretion. On top of this dark matter physics, we layer our understanding of gas cooling, star formation, and feedback. We know that our current prescriptions for these processes are vastly oversimplified, but hope to learn about how these processes operate – when averaged over entire galaxies – by comparison to observations.

Because the overall process is stochastic, some of the most important tests of the models are against large statistical data sets. These data sets must be uniform, with known, well-defined selection functions. SDSS has demonstrated the power of such large-area surveys, and we can anticipate further progress from SkyMapper, PS1, DES, and other surveys before LSST comes on line. There will also undoubtedly be progress in smaller-area deep surveys following on from the Hubble Deep Fields, GOODS, COSMOS, and the Subaru Deep Fields.

LSST will be a unique tool to study the universe of galaxies. The database will provide photometry for 10^{10} galaxies, from the local group to redshifts $z > 6$. It will provide useful shape measurements and six-band photometry for about 4×10^9 galaxies (§ 3.7.2). Figure 9.1 and Figure 9.2 provide indications of the grasp of LSST relative to other existing or planned surveys.

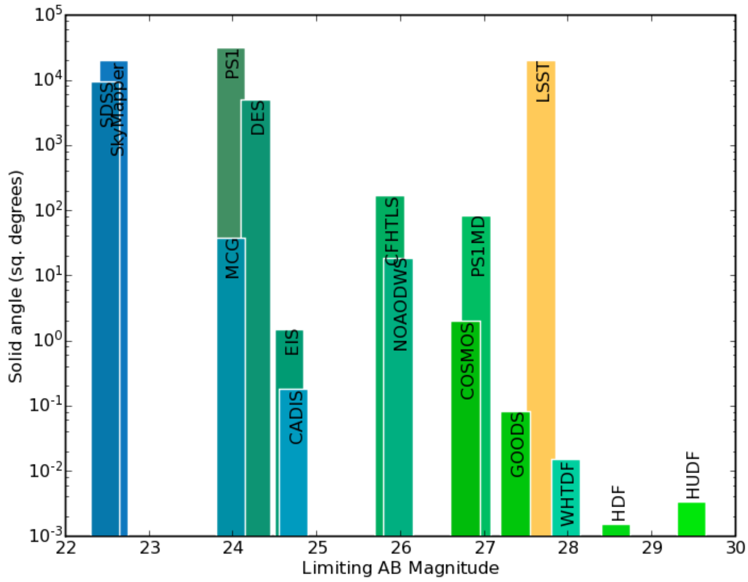

Figure 9.1: Comparison of survey depth and solid angle coverage. The height of the bar shows the solid angle covered by the survey. The color of the bar is set to indicate a combination of resolution, area, and depth with rgb values set to $r = V/V(\mathrm{HUDF})$, $g = (m_{\mathrm{lim}} - 15/)/16$, and $b = \theta/2''$, where V is the volume within which the survey can detect a typical L^* galaxy with a Lyman-break spectrum in the r band, m_{lim} is the limiting magnitude, and θ is the resolution in arcseconds. The surveys compared in the figure are as follows: SDSS: Sloan Digital Sky Survey; MGC: Millennium Galaxy Catalog (Isaac Newton Telescope); PS1: PanSTARRS-1 wide survey, starting in 2009 in Hawaii; DES: Dark Energy Survey (Cerro-Tololo Blanco telescope starting 2009); EIS: ESO Imaging survey (complete); CADIS: Calar Alto Deep Imaging Survey; CFHTLS: Canada France Hawaii Telescope Legacy Survey; NOAODWS: NOAO Deep Wide Survey; COSMOS: HST 2 deg^2 survey with support from many other facilities; PS1MD: PanSTARRS-1 Medium-Deep Survey covering 84 deg^2; GOODS: Great Observatories Origins Deep Survey (HST, Spitzer, Chandra, and many other facilities); WHTDF: William Herschel Telescope Deep Field; HDF, HUDF: Hubble Deep Field and Ultra Deep Field.

A key to testing our understanding of galaxy formation and evolution will be to examine the full multi-dimensional distributions of galaxy properties. Tools in use today include the luminosity function of galaxies, the color-luminosity relation, size-luminosity relation, quantitative morphology, and the variation of these distributions with environment (local density or halo mass). As data sets and techniques evolve, models will be tested not just by their ability to reproduce the mean trends but by their ability to reproduce the full distribution in multiple dimensions. Studies of the tails of these distributions – e.g., galaxies of unusual surface brightness or morphology – give us the leverage to understand short-lived phases of galaxy evolution and to probe star formation in a wide range of environments.

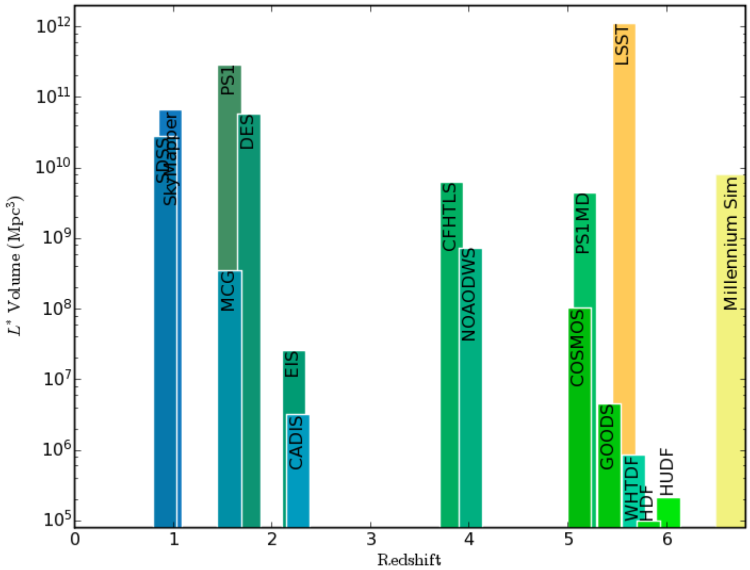

Figure 9.2: Co-moving volume within which each survey can detect a galaxy with a characteristic luminosity L^* ($M_B \sim -21$) assuming a typical Lyman-break galaxy spectrum. LSST encompasses about two orders of magnitude more volume than current or near-future surveys or the latest state-of-the-art numerical simulations. This figure shows the same surveys as the previous diagram, with the addition of the Millennium Simulation (Springel et al. 2005).

The core science of the Galaxies Science Collaboration will consist of measuring these distributions and correlations as a function of redshift and environment. This will make use of the all-sky survey and the deep fields. Accurate photometric redshifts will be needed, as well as tools to measure correlation functions, and catalogs of clusters, groups, overdensities on various scales, and voids, both from LSST and other sources.

The layout of this chapter is as follows. We begin (§ 9.2) by outlining the measurements and samples that will be provided by LSST. We then focus on topics that emphasize counting objects as a function of redshift, proceeding from detection and characterization of objects to quantitative measurements of evolutionary trends (§ 9.3-§ 9.9). In § 9.5, we turn to environmental studies, beginning with an outline of the different types of environment and how they can be identified with LSST alone or in conjunction with other surveys and discussing measurements that can be carried out on the various environment-selected galaxy catalogs. We conclude in § 9.11 with a discussion of public involvement in the context of galaxy studies.

9.2 Measurements

Over the $\sim$ 12 billion years of lookback time accessible to LSST, we expect galaxies to evolve in luminosity, color, size, and shape. LSST will not be the deepest or highest resolution survey in existence. However, it will be by far the largest database. It will resolve scales of less than $\sim$ 3 kpc at any redshift. It is capable of detecting typical star-forming Lyman-break galaxies $L > L^*$ out to $z > 5.5$ and passively evolving $L > L*$ galaxies on the red sequence out to $z \sim 2$ over 20,000 deg^2. For comparison, the combined area of current surveys to this depth available in 2008 is less than 2 deg^2. In deep drilling fields (§ 2.1), the LSST will go roughly ten times deeper over tens of square degrees. The basic data will consist of positions, fluxes, broad-band spectral energy distributions, sizes, ellipticities, position angles, and morphologies for literally billions of galaxies (§ 3.7.2). Derived quantities include photometric redshifts (§ 3.8), star-formation rates, internal extinction, and stellar masses.

9.2.1 Detection and Photometry

The optimal way to detect an object of a known surface brightness profile is to filter the image with that surface brightness profile, and apply a S/N threshold to that filtered image. In practice, this is complicated by the wide variety of shapes and sizes for galaxies, combined with the fact that they can overlap with each other and with foreground stars. The LSST object catalog will be a compromise, intended to enable a broad spectrum of scientific programs without returning to the original image data.

Perhaps the most challenging aspect of constructing a galaxy catalog is the issue of image segmentation, or deblending. Galaxies that are either well resolved, or blended with a physical neighbor or a chance projection on the line-of-sight can be broken into sub-components (depending on the S/N and PSF). Improperly deblending overlaps can result in objects with unphysical luminosities, colors, or shapes. Automated deblending algorithms can be quite tricky, especially when galaxies are irregular or have real substructure (think of a face-on Sc in a dense stellar field). It will be important to keep several levels of the deblending hierarchy in the catalog, as well as have an efficient way to identify close neighbors. Testing and refining deblending algorithms is an important aspect of the near-term preparations for LSST.

9.2.2 Morphology

The excellent image quality that LSST will deliver will allow us to obtain morphological information for all the extended objects with sufficient signal-to-noise ratio, using parametric model fitting and non-parametric estimation of various morphology indices. The parametric models, when the PSF is properly accounted for, will produce measurements of the galaxy axial ratio, position angle and size. Possible models are a general Sersic model and more classical bulge and disk decomposition. In the case of an $r^{1/4}$−law, the size corresponds to the bulge effective radius, while for an exponential disk, it is the disk scale-length. This process naturally produces a measurement of the object surface brightness, either central or median. An example of such a fit is shown in Figure 9.3 (Barrientos et al. 2004).

The median seeing requirement of $0.7''$ corresponds to ~ 4 kpc at $z = 0.5$, which is smaller than a typical L^* galaxy scale-length. Therefore, parametric models will be able to discriminate between bulge or disk dominated galaxies up to $z \sim 0.5 - 0.6$, and determine their sizes for the brightest ones. Non-parametric morphology indicators include concentration, asymmetry, and clumpiness

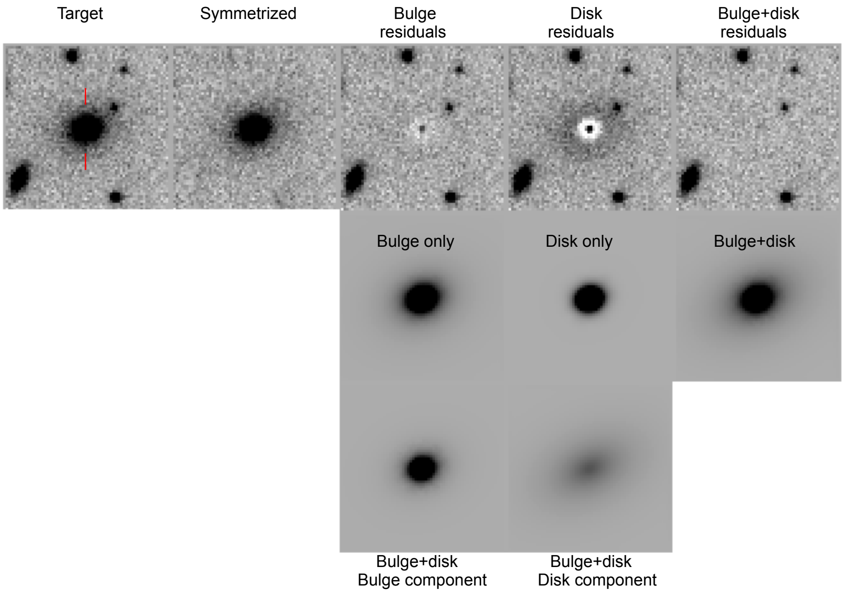

Figure 9.3: Example of two-dimensional galaxy light profile fitting. The top left panel corresponds to the target galaxy, the next to the right is its symmetrized image, the next three show the residuals from bulge, disk, and bulge plus disk models respectively. The corresponding models are shown in the lower panel, with the bulge and disk (of the bulge plus disk model) components in the third row. This galaxy is best fit by an $r^{1/4}-$law or a bulge plus disk model.

(CAS; Conselice 2003) as well as measures of the distribution function of galaxy pixel flux values (the Gini coefficient) and moments of the galaxy image (M_{20}; Lotz et al. 2004).

9.3 Demographics of Galaxy Populations

It is useful for many purposes to divide galaxies into different classes based on morphological or physical characteristics. The boundaries between these classes are often fuzzy, and part of the challenge of interpreting data is ensuring that the classes are defined sensibly so that selection effects do not produce artificial evolutionary trends. Increasingly realistic simulations can help to define the selection criteria to avoid such problems. Here we briefly discuss the detectability of several classes of galaxies of interest for LSST. We shall discuss the science investigations in more depth later in this chapter.

Passively evolving galaxies. Early-type galaxies, with little or no star formation, represent roughly one-half of the present day stellar mass density (Bell et al. 2003). These galaxies formed their stars earlier and more rapidly than late-type galaxies. They are more strongly clustered. It is likely that mergers played an important role in their formation, contributing to their rapid star formation rates and their kinematically hot structure. It is also likely that some form of feedback or "strangulation" prevented the subsequent accretion and cooling of gas that would have led to further star formation. With good sensitivity in the i, z, and y bands, LSST will be sensitive to L^* early-type galaxies out to redshifts $z \sim 2$ for the wide area survey, and, depending on observing

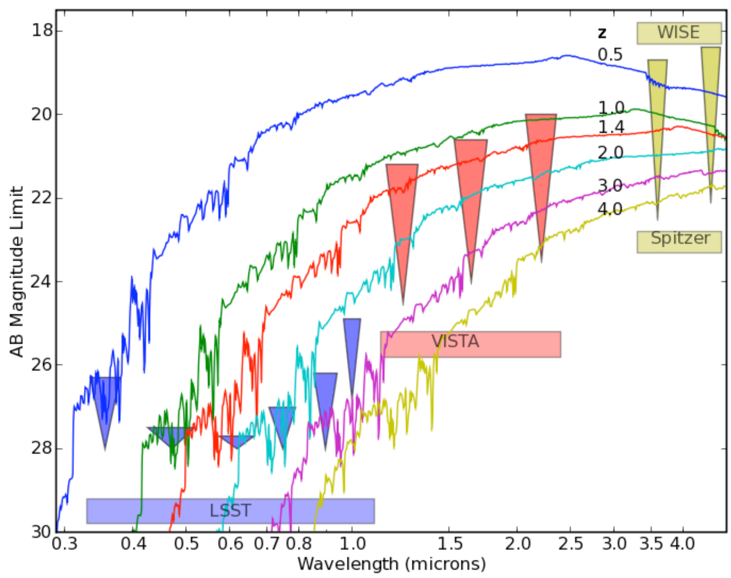

Figure 9.4: The spectrum of a fiducial red-sequence galaxy as a function of redshift. The spectral energy distribution is from a Maraston (2005) model, with solar metallicity, Salpeter IMF, with a star formation timescale of 0.1 Gyr, beginning to form stars at $z = 10$, and normalized to an absolute B_{AB} mag of -20.5 at $z = 0$. Magnitude limits are indicated as blue triangles in the optical for LSST, red triangles in the near-IR for VISTA and yellow triangles in the mid-IR for Spitzer and WISE. The wide top of the triangle shows the limits corresponding to surveys of roughly 20,000 deg^2 (the VISTA Hemisphere Survey, and the WISE all-sky survey). The point of the triangle corresponds to depths reached over tens of square degrees. For LSST we use a strawman for the deep drilling fields (§ 2.1) that corresponds to putting 1% of the time into each field (i.e., 10% if there are 10 separate fields). Apportioning the time in these fields at $9, 1, 2, 9, 40, 39\%$ in *ugrizy* yields 5σ point source detection depths of $28.0, 28.0, 28.0, 28.0, 28.0, 26.8$, which is what is shown. For VISTA the deep fields correspond to the VIDEO survey; for Spitzer they correspond to SWIRE.

strategy, to $z \sim 3$ for the deep-drilling fields. Figure 9.4 shows the LSST survey limits compared to a passively-evolving L^* early type galaxy.

High-redshift star forming galaxies. In the past decade or so, deep surveys from the ground and space have yielded a wealth of data on galaxies at redshifts $z > 2$. Photometric sample sizes have grown to $> 10^4$ galaxies at $z \sim 3$ and $> 10^3$ galaxies at $z > 5$. (Spectroscopic samples are roughly an order of magnitude smaller.) However, we still have only a rudimentary understanding of how star formation progresses in these galaxies, we do not know how important mergers are, we and have only very rough estimates of the relations between galaxy properties and halo mass. LSST will provide data for roughly 10^9 galaxies at $z > 2$, of which $\sim 10^7$ will be at $z > 4.5$. Detection limits for LSST compared to a fiducial evolving L^* Lyman break galaxy are shown in Figure 9.5.

Dwarf galaxies. LSST will be very useful for studies of low luminosity galaxies in the nearby Universe. Blind H I surveys and slitless emission-line-galaxy surveys have given us reasonable constraints on the luminosity function and spatial distribution of gas-rich, star forming galaxies. However, most of the dwarfs in the local group lack H I or emission lines. Such dE or dSph galaxies tend to have low surface brightnesses (§ 9.6) and are difficult to find in shallow surveys like the

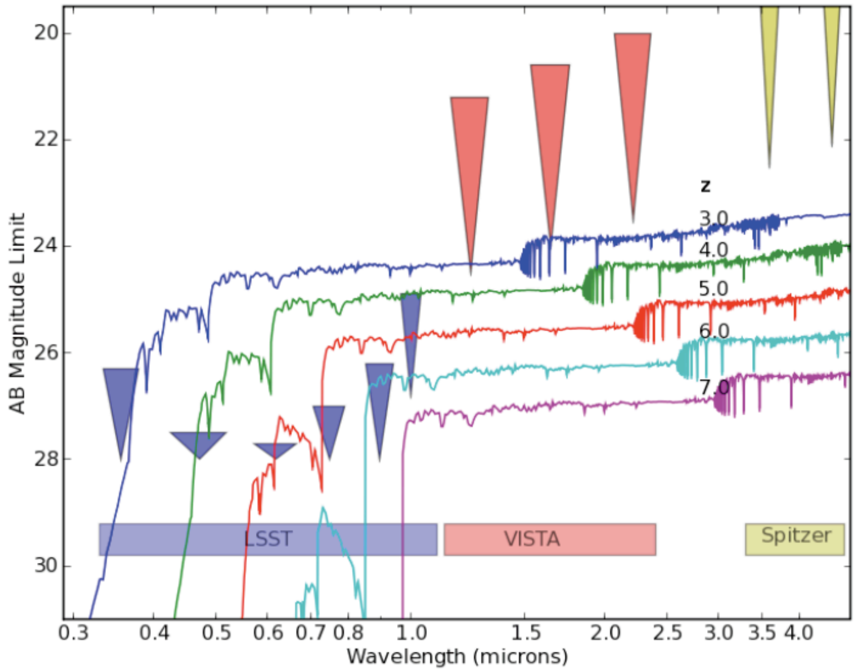

Figure 9.5: Fiducial Lyman-break galaxy as a function of redshift. The spectral energy distribution is a Bruzual & Charlot (2003) model, with solar metallicity, a Salpeter IMF, an age of 0.2 Gyr and a constant star formation rate, viewed through a Calzetti et al. (2000) extinction screen with $E(B-V) = 0.14$ (Reddy et al. 2008). This is normalized to an absolute AB mag at 1600 Å of $-20.97, -20.98, -20.64, -20.24$, and -19.8 at $z = 3, 4, 5, 6$, and 7 respectively (Reddy & Steidel 2009; Bouwens et al. 2008). Magnitude limits are the same as those shown in Figure 9.4.

SDSS or 2MASS, and are also difficult targets for spectroscopy. Our census of the local Universe is highly incomplete for such galaxies. Figure 9.6 shows some typical example morphologies. Figure 9.7 shows the magnitude–radius relation for dwarf galaxies at a variety of distances. Nearby dwarf galaxies within a few Mpc and distant faint galaxies are well-separated in this space; their low photometric redshifts will further help to distinguish them. An important question will be the extent to which systematic effects in the images (scattered light, sky subtraction issues, deblending, flat-fielding) will limit our ability to select these low surface brightness galaxies.

Mergers and interactions. The evolution of the galaxy merger rate with time is poorly constrained, with conflicting results in the literature. LSST will provide an enormous data set not only for counting mergers as a function of redshift, but also for quantifying such trends as changes in color with morphology or incidence of AGN versus merger parameters. LSST is comparable to the CFHTLS-Deep survey in depth, wavelength coverage, seeing, and plate scale — but covers an area 5000× larger. Scaling from CFHTLS, we expect on the order of 15 million galaxies will have detectable signs of strong tidal interactions. At low redshift, LSST will be useful for detecting large-scale, low surface brightness streams, which are remnants of disrupted dwarf galaxies (§ 9.9).

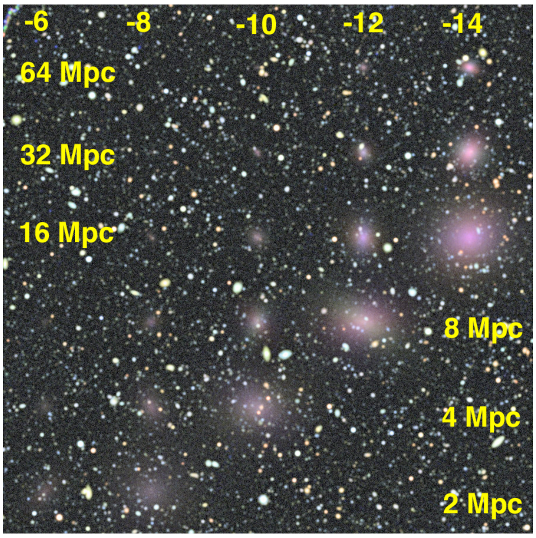

Figure 9.6: Dwarf spheroidal galaxy visibility. Dwarfs of various distances and absolute magnitudes have been inserted into a simulated LSST image. The simulation is for 50 visits (1500s) each in dark time with g, r, i. The background image is from the GOODS program (Giavalisco et al. 2004), convolved with a 0.7″ PSF with appropriate noise added. Sizes and colors for the dwarfs are computed from the size-magnitude and mass-metallicity relations of Woo et al. (2008) assuming a 10-Gyr old population.

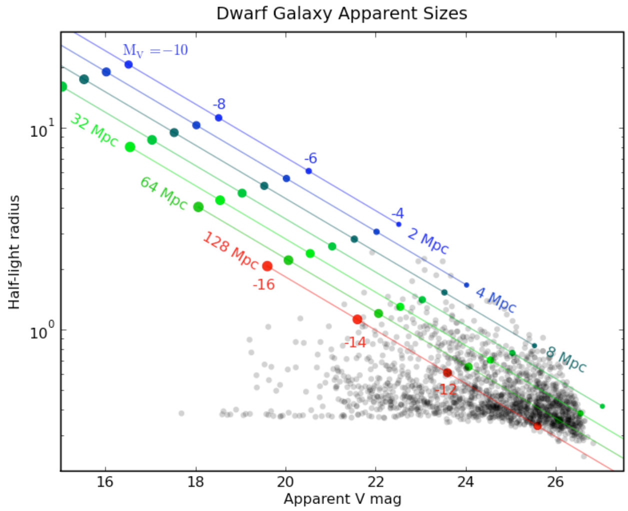

Figure 9.7: The colored points and lines show the half-light radii in arcsec for dwarf galaxies as a function of magnitude for distances ranging from 2 to 128 Mpc computed from the scaling relation of Woo et al. (2008). The gray points show the sizes of typical background galaxies measured from the simulation in Figure 9.6. A dwarf galaxy with $M_V = -4$ should be visible and distinguishable from the background out to ~ 4 Mpc; a dwarf with $M_V = -14$ at 128 Mpc will be larger than most of the background galaxies of the same apparent magnitude.

9.4 Distribution Functions and Scaling Relations

One of the key goals of the Galaxy Science Collaboration is to measure the multivariate properties of the galaxy population including trends with redshift and environment. This includes observed galaxy properties, including luminosities, colors, sizes, and morphologies, as well as derived galaxy properties, including stellar masses, ages, and star formation rates, and how the joint distribution of these galaxy properties depends on redshift and environment as measured on a wide range of scales.

Galaxy formation is inherently stochastic, but is fundamentally governed (if our theories are correct) by the statistical properties of the underlying dark matter density field. Determining how the multivariate galaxy properties and scaling relations depend on this density field, and on the underlying distribution and evolution of dark matter halos, is the key step in connecting the results of large surveys to theoretical models of structure formation and galaxy formation. We describe this dark matter context further in the following section.

A complete theory of galaxy formation should reproduce the fundamental scaling relations of galaxies and their scatter as a function of redshift and environment, in the high dimensional space of observed galaxy properties. Unexplained scatter, or discrepancies in the scaling relations, signals missing physics or flaws in the model. We need to be able to subdivide by galaxy properties and redshift with small enough errors to quantify evolution at a level compatible with the predictive capability of the next generation of simulations. By going both deep and wide, LSST is unique in its ability to quantify the global evolution of the multivariate distribution galaxy properties.

Indeed, the consistency of these properties (e.g., the luminosity function in different redshift slices) across the full survey may well be an important cross-check of calibration and photometric redshift accuracy. The massive statistics may reveal subtle features in these distributions, which in turn could lead to insight into the physics that governs galaxy evolution.

9.4.1 Luminosity and Size Evolution

The tremendous statistics available from billions of galaxies will allow the traditional measures of galaxy demographics and their evolution to be determined with unprecedented precision. The luminosity function, $N(L)\,dL$, gives the number density of galaxies with luminosity in the interval $[L, L+dL]$. It is typically parametrized by a Schechter (1976) function. LSST data will enable us to measure the luminosity functions of all galaxy types at all redshifts, with the observed bands corresponding to rest-frame ultraviolet-through-near-infrared at low redshift ($z < 0.3$), rest-frame ultraviolet-to-optical at moderate redshift ($0.3 < z < 1.5$), and rest-frame ultraviolet at high redshift ($z > 1.5$). We will also determine the color distribution of galaxies in various redshift bins, where color is typically measured as the difference in magnitudes in two filters e.g., $g - r$, and this has a direct correspondence to the effective power law index of a galaxy's spectrum in the rest-frame optical. Color reveals a combination of the age of a galaxy's stellar population and the amount of reddening caused by dust extinction, and we will use the great depth of LSST data to expand studies of the galaxy color-morphology relation to higher redshift and lower luminosity. Image quality of $0.7''$ in deep r-band images will allow us to measure the sizes of galaxies (typically parametrized by their half-light or effective radii) out to $z \sim 0.5$ and beyond. Size studies at higher redshift are hampered by the nearly unresolved nature of galaxies caused by the gradual decrease in galaxy sizes with redshift and the increase in angular diameter distance until its plateau at $z > 1$. Nevertheless, LSST will provide unique data on the incidence of large galaxies at high redshifts, which may simply be too rare to have appeared in any great quantity in existing surveys.

9.4.2 Relations Between Observables

Broadly speaking, galaxies fall into two populations, depending on their mass and their current star formation rate (Kauffmann et al. 2003; Bell et al. 2004). Massive galaxies generally contain old, passively evolving stellar populations, while galaxies with ongoing star formation are less massive. This bimodality is clearly expressed in color-magnitude diagrams. Luminous galaxies populate a tight red sequence, and star forming ones inhabit a wider and fainter blue cloud, a landscape that is observed at all times and in all environments from the present epoch out to at least $z \sim 1$.

The origin of this bimodality, and particularly of the red sequence, dominates much of the present discussion of galaxy formation. The central questions include: 1) what path in the color-magnitude diagram do galaxies trace over their evolutionary history? 2) what physical mechanisms are responsible for the necessary "quenching" of star formation which may allow galaxies to move from the blue cloud to the red sequence? and 3) in what kind of environment do the relevant mechanisms operate during the passage of a typical galaxy from the field into groups and clusters? Answering the first question would tell us whether galaxies are first quenched, and then grow in mass *along* the red sequence (e.g., by dry mergers, in which there are no associated bursts of star formation), or grow primarily through star formation and then quench directly onto their final position on the red sequence (see e.g., Faber et al. 2007). The latter two issues relate more specifically to galaxy clusters and dense environments in general. We know that galaxies move more quickly to the red sequence in denser environments – the red sequence is already in place in galaxy clusters by $z \sim 1.5$ when it is just starting to form in the field. So by studying the full range of environments we should be able to make significant advances in answering the central questions.

Because a small amount of star formation is enough to remove a galaxy from the red sequence, it is of great interest to quantify the distribution of galaxy colors near the red sequence, in multiple bands, and in multiple environments. This should allow us to make great progress in distinguishing bursty and episodic star formation from star formation that is being slowly quenched.

Blanton et al. (2003, 2005) have looked at the paired relations between photometric quantities in the SDSS, and such relations have provided insights into the successes and failures of the current generation of galaxy evolution models (Gonzalez et al. 2008). LSST will push these relations to lower luminosities and surface brightnesses and reveal trends as a function of redshift with high levels of statistical precision.

The physical properties of galaxies can be more tightly constrained when LSST data are used in conjunction with data from other facilities. For high-redshift galaxies, the rest-frame ultraviolet luminosity measured by LSST reveals a combination of the "instantaneous" star formation rate (averaged over the past ~ 10 Myr) and the dust extinction; the degeneracy is broken by determining the dust extinction from the full rest-ultraviolet-through-near-infrared spectral energy distribution (SED) and/or by revealing the re-radiation of energy absorbed by dust at far-infrared-to-millimeter wavelengths. At lower redshifts, LSST probes the stellar mass, stellar age, and dust extinction at rest-frame optical wavelengths, and degeneracies can be mitigated using the full rest-ultraviolet-through-near-infrared SED to measure stellar mass. Luminosities in additional wavebands such as $L_X, L_{\rm NIR}, L_{\rm MIR}, L_{\rm FIR}, L_{\rm mm}$, and $L_{\rm radio}$ can be added to the distribution function, revealing additional fundamental quantities including the AGN accretion rate, dust mass, and dust temperature. Because most surveys that are deep enough to complement LSST will cover much smaller area, coordinating the locations of the LSST deep fields to maximize the overlap with other facilities will be important.

9.4.3 Quantifying the Biases and Uncertainties

Because much of the power of LSST for galaxies will come from the above-mentioned statistical distributions, it will be crucial to quantify the observational uncertainties, biases, and incompleteness of these distributions. This will be done through extensive simulations (such as those in Figure 9.6), analyzed with the same pipelines and algorithms that are applied to real data. The results of these simulations can be used to construct transfer functions, which simultaneously capture uncertainties, bias and incompleteness as a function of the input model properties of the galaxies. A given galaxy image will suffer from different noise and blending issues depending on where it falls in which images with which PSFs. With thousands of realizations sampling the observational parameter space of galaxies, one can build a smooth representation of the probability distribution of recovered values with respect to the input parameters, and thus quantify errors and biases. The deep drilling fields can be used to validate these transfer functions for the wide-deep survey. These probability distributions can then be used when trying to derive true scaling relations from the LSST data or to compare LSST data to theoretical predictions.

9.5 Galaxies in their Dark-Matter Context

In the modern galaxy formation paradigm, set in the context of ΛCDM, structure forms hierarchically from small to large scales. Galaxies are understood to form at the densest peaks in this hierarchical structure within bound dark matter structures (halos and subhalos). The properties of galaxies themselves are determined by the physics of gas within the very local overdensity that forms the galaxy (which depends on density, metallicity, and angular momentum), and on the interactions between that specific overdensity and the nearby overdensities (mergers, tides, and later incorporation into a larger halo). For instance, the dark matter dominates the potential well depth and hence the virial temperature of a halo, which sets the equilibrium gas temperature, determining whether infalling material can cool efficiently and form stars (Silk 1977; Rees & Ostriker 1977; Binney 1977; White & Rees 1978; Kereš et al. 2009; Dekel et al. 2009). Similarly, galaxy properties can change radically during mergers; and the merger history of a galaxy is also intimately related to the merger history of its underlying halo, which can be very different in halos of different masses (e.g., Lacey & Cole 1993, Wechsler et al. 2002).

Connecting galaxies to their underlying dark matter halos allows one to understand their cosmological context, including, in a statistical sense, their detailed merging and formation histories. These relationships are not merely theoretical; the distribution of galaxy properties changes radically from the low-mass, high star formation rate galaxies near cosmic voids, where halo masses are low, to the quiescent, massive early-type galaxies found in the richest clusters, where dark matter halo masses are very high.

9.5.1 Measuring Galaxy Environments with LSST

One way of exploring these relationships is to measure the variation of galaxy properties as a function of the environment in which a galaxy is found (e.g., cluster vs. void), using the local overdensity of galaxies as a proxy for the local dark matter density. However, environment measures for individual galaxies are noisy even with spectroscopic samples, due to sparse sampling and the increase of peculiar velocities in dense environments; a solution is to measure the average overdensity of galaxies as a function of their properties (Hogg et al. 2003), a formulation which minimizes errors and bin-to-bin correlations. The situation is much worse for photometric samples, as simulations demonstrate that local overdensity is very poorly determined if only photometric redshifts are available (Cooper et al. 2005). The problem is straightforward to see: the characteristic size of clusters is $\sim 1h^{-1}$ Mpc co-moving, and the characteristic clustering scale length of galaxies is $\sim 4h^{-1}$ Mpc co-moving for typical populations of interest, but even a photometric redshift error as small as 0.01 in z at $z = 1$ corresponds to an 18 h^{-1} Mpc error in co-moving distance.

As a consequence, with photometric redshifts alone it is *impossible* to determine whether an *individual object* is inside or outside a *particular structure*. Hence, just as with spectroscopic surveys, it is far more robust to measure the *average overdensity as a function of galaxy properties*, rather than *galaxy properties as a function of overdensity*. This may seem like an odd thing to do - after all, we tend to think of mechanisms that affect a galaxy associated with a particular sort of environment – but in fact, a measurement of average overdensity is equivalent to a measurement of the *relative large-scale structure bias* of a population – a familiar way of studying the relationship between galaxies and the underlying dark matter distribution.

There are a variety of methods we will apply for this study. Simply counting the average number of neighbors a galaxy has (within some radius and Δz) as a function of the central galaxy's properties, will provide a straightforward measure of overdensity analogous to environment measures used for spectroscopic surveys (Hogg et al. 2003; Cooper et al. 2006). This idea is basically equivalent to measuring the cross-correlations between galaxies (as a function of their properties) and some tracer population, a technique that can yield strong constraints on the relationship between galaxies and the underlying dark matter (§ 9.5.4).

These cross-correlation techniques can even be applied to study galaxy properties as a function of environment, rather than the reverse: given samples of clusters (or voids) in LSST, we can determine their typical galaxy populations by searching for excess neighbors around them with a particular set of galaxy properties. Such techniques (analogous to stacking the galaxy populations around a set of clusters) have a long history (e.g., Oemler 1974; Dressler 1980; more recently Hansen et al. 2009), but will have unprecedented power in LSST data thanks to the accurate photometric redshifts (reducing contamination), great depth (allowing studies deep into the luminosity function), and the richness of galaxy properties to be measured.

9.5.2 The Galaxy–Halo Connection

Given our knowledge of the background cosmology (e.g., at the pre-LSST level, assuming that standard dark energy models are applicable, Appendix A), we can calculate the distribution of dark matter halo masses as a function of redshift (Tinker et al. 2008), the clustering of those halos (Sheth et al. 2001), and the range of assembly histories of a halo of a given mass (Wechsler et al. 2002). Both semi-analytic methods and N-body simulations can predict these quantities, with excellent agreement. Uncertainties in the processes controlling galaxy evolution are currently much greater than the uncertainties in the modeling of dark matter.

What is much less constrained now, and almost certainly will still be unknown in many details in the LSST era, is how *visible* matter relates to this underlying network of dark matter. It is in general impossible to do this in an object-by-object manner (except in cases of strong gravitational lensing, Chapter 12), but in recent years there has been considerable success in determining how many galaxies of given properties will be found in a halo of a given dark matter mass (e.g., Bullock et al. 2002; Zehavi et al. 2004; van den Bosch et al. 2007; Yang et al. 2008; Zheng et al. 2007; Conroy & Wechsler 2009).

The connection between a population of galaxies and dark matter halos can be specified by its halo occupation distribution (or HOD) (Berlind & Weinberg 2002), which specifies the probability distribution of the number of objects of a given type (e.g., luminosity, stellar mass, color, or star formation rate) and their radial distribution given the properties of the halo, such as its mass (and/or formation history). The HOD and the halo model have provided a powerful theoretical framework for quantifying the connection between galaxies and dark matter halos. They represent a great advance over the linear biasing models used in the past, which assume that the clustering properties of some population of interest will simply be stronger than the clustering of dark matter by a constant factor at all scales.

In the simplest HOD model, the multiplicity function $P(N|M)$ (the probability distribution of the number of subhalos found within halos of mass M) is set by the dark matter (Kravtsov et al. 2004), and the details of galaxy star formation histories map this multiplicity function to a conditional luminosity function, $P(L|M)$. This deceptively simply prescription appears to be an excellent description of the data (van den Bosch et al. 2003; Zheng et al. 2005; Cooray 2006; van den Bosch et al. 2007). A variety of recent studies have also found that this approach can be greatly simplified with a technique called abundance matching, in which the most massive galaxies are assigned to the most massive halos monotonically (or with a modest amount of scatter). This technique has also been shown to accurately reproduce a variety of observational results including various measures of the redshift– and scale–dependent spatial clustering of galaxies (Colín et al. 1999; Kravtsov et al. 2004; Conroy et al. 2006; Vale & Ostriker 2006).

There are several outstanding issues. In the HOD approach, it is unclear whether the galaxy distribution can be described solely by properties of the halo mass, or whether there are other relevant halo or environmental properties that determine the galaxy populations. Most studies to date have considered just one galaxy property (e.g., luminosity or stellar mass). With better observations, the HOD approach can be generalized to encompass the full range of observed properties of galaxies. Instead of the conditional luminosity function $P(L|M)$ at a single epoch, we need to be considering multi-dimensional distributions that capture the galaxy properties we would like to explain and the halo properties that we believe are relevant: $P(L, a, b, c, ...|M, \alpha, \beta, \gamma, ...)$, where $a, b, c, ...$ are parameters such as age, star formation rate, galaxy type, etc., and $\alpha, \beta, \gamma, ...$ are parameters of the dark-matter density field such as overdensity on larger scales or shape.

Measuring the distributions of galaxy properties (§ 9.4) and their relationship to environment (i.e., average overdensity) and clustering (§ 9.5.4) measurements on scales ranging from tens of kiloparsecs to hundreds of Megaparsecs will allow us to place strong constraints on this function, determining the relationship between galaxy properties and dark matter, which will be key for testing theories of galaxy evolution and for placing galaxies within a cosmological context. In addition to providing an unprecedentedly large sample, yielding high precision constraints, LSST will be unique in its ability to determine the dark matter host properties for even extremely rare populations of galaxies. We describe several of the techniques we can apply to LSST data to study the relationship between galaxies and dark matter in the remainder of this section. In general, they are applicable to almost any galaxy property that can be measured for a sample of LSST galaxies, and thus together they give extremely powerful constraints on galaxy formation and structure formation models.

9.5.3 Clusters and Cluster Galaxy Evolution

The large area and uniform deep imaging of LSST will allow us to find an unprecedented number of galaxy clusters. These will primarily be out to $z \sim 1.3$ where the LSST optical bands are most useful, although additional information can be obtained using shear-selected peaks out to substantially higher redshift (Abate et al. 2009). This new sample of clusters will be an excellent resource for galaxy evolution studies over a wide redshift range. LSST will allow studies of the galaxy populations within hundreds of $\sim 1 \times 10^{15} M_\odot$ clusters as well as hundreds of thousands of intermediate mass clusters at $z > 1$. For a discussion of cluster-finding algorithms, the use of clusters as a cosmological probe and estimates of sample sizes, see § 13.6 and § 12.12.

Of particular interest will be the study of the red sequence populated by early type galaxies, which is present in essentially all rich clusters today. This red sequence appears to be in place in at least some individual clusters up to $z \sim 1.5$. As an example, Figure 9.8 shows that the red sequence is already well defined in the cluster RDCS1252.9-2927 at $z = 1.24$. The homogeneity in the colors for this galaxy population indicates a high degree of coordination in the star formation histories for the galaxies in this cluster. In general however, the role of the galaxy cluster environment in the evolution of its member galaxies is not yet well understood. Issues include on what timescale and with what mechanism the cluster environment quenches star formation and turns galaxies red, and how this relation evolves with cosmic time.

Galaxy populations in a photometric survey can be studied using the cross-correlation of galaxies with clusters, allowing a full statistical characterization of the galaxy population as a function of cluster mass and cluster-centric radius, and avoiding many of the issues with characterizing galaxy environment from photometric redshift surveys. This has been applied with much success to the photometric sample of the SDSS (Hansen et al. 2009), where excellent statistics have allowed selecting samples, which share many common properties (e.g., by color, position, and whether central or satellite) to isolate different contributions to galaxy evolution. Although such studies will be substantially improved by pre-LSST work e.g., from DES, LSST will be unique in a few respects: 1) studies of the galaxy population for the most massive clusters above $z \sim 1$; 2) studies of faint galaxies in massive clusters for a well-defined sample from $z \sim 1.3$ to the present; and 3) studies of the impact of large scale environment on the galaxy population. At lower redshifts or with the aid of follow-up high-resolution imaging, LSST will also allow these studies to be extended to include galaxy morphology information, so that the morphological Butcher-Oemler effect (Goto et al. 2004) can be studied as a function of redshift for large samples over a wide luminosity range.

We are only beginning to systematically examine the outskirts of clusters and their infalling groups at moderate redshifts, and this effort will most likely be ongoing when LSST begins operations. LSST will be able to produce significant gains over the state of cluster research in the middle of the next decade by focusing on the interface regions between cluster cores, groups, and superclusters. These areas are particularly hard to study currently because the galaxy densities are too low for targeted spectroscopic follow-up, and large area spectroscopic studies do not cover enough volume at moderate redshifts to effectively sample the relatively rare supercluster type environments.

9.5.4 Probing Galaxy Evolution with Clustering Measurements

The parameters of halo occupation models of galaxy properties (described in § 9.5.2) may be established by measuring the clustering of the population of galaxies of interest. This may be a sample of galaxies selected from LSST alone or in concert with photometry at other wavelengths. The principal measure of clustering used is the two-point correlation function, $\xi(r)$: the excess probability over the expectation for a random, unclustered distribution that one object of a given

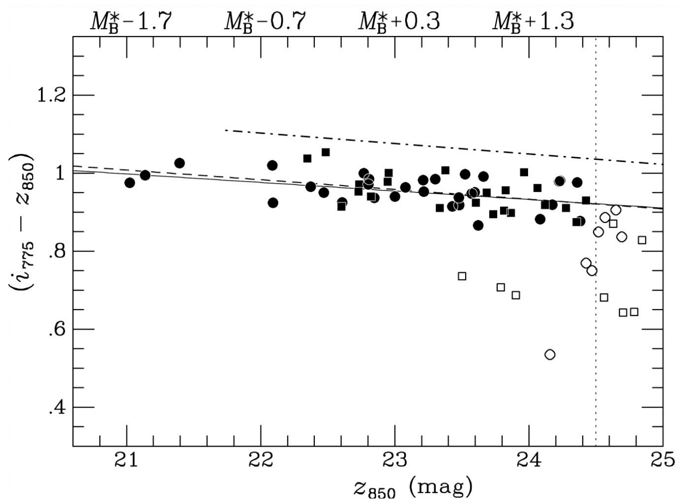

Figure 9.8: Color-magnitude diagram for the cluster RDCS1252-2927 at $z = 1.24$ (Blakeslee et al. 2003). A color-magnitude diagram of this quality will be achieved with LSST in a single visit in two bands.

class will be a distance r away from another object in that class. This function is generally close to a power law for observed populations of galaxies, $\xi(r) = (r/r_0)^{-\gamma}$, for some scale length r_0, typically $\sim 3 - 5h^{-1}$ Mpc co-moving for galaxy populations of interest, and slope γ, typically in the range 1.6–2. However, there is generally a weak break in the correlation function corresponding to the transition between small scales (where the clustering of multiple galaxies embedded within the same dark matter halos is observed, the so-called "one-halo regime") to large scales (where the clustering between galaxies in different dark matter halos dominates, the "two-halo regime"). The more clustering properties are measured (e.g., higher-order correlation functions or redshift-space distortions, in addition to projected two-point statistics), the more precisely the parameters of the relevant halo model may be determined (Zehavi et al. 2004; Tinker et al. 2008).

Measuring Angular Correlations with LSST

While models predict the real-space correlation function, $\xi(r)$, for a given sample, we are limited to photometric redshifts, and thus we we will measure the angular two-point auto-correlation function $w(\theta)$: the excess probability over random of finding a second object of some class (e.g., selected in a slice in photometric redshift) an angle θ away from the first one. Given modest assumptions, the value of $w(\theta)$ can be determined from knowledge of $\xi(r)$ through Limber's Equation (Limber 1953; Peebles 1980):

$$w(\theta) = \frac{\int d\bar{z} \left(\frac{dN}{d\bar{z}}\right)^2 \int dl \, \xi(r(\theta, l), \bar{z})}{\left(\int \frac{dN}{dz} \, dz\right)^2}, \tag{9.1}$$

where dN/dz is the redshift distribution of the sample (which may have been selected, e.g., by photometric redshifts, to cover a relatively narrow range), l is the co-moving separation of two objects along the line of sight, and $\bar{z}$ is their mean redshift. The quantity $r \approx (D_c^2\theta^2 + l^2)^{1/2}$, where D_c is the co-moving angular size distance. The amplitude of w will increase proportionally as ξ

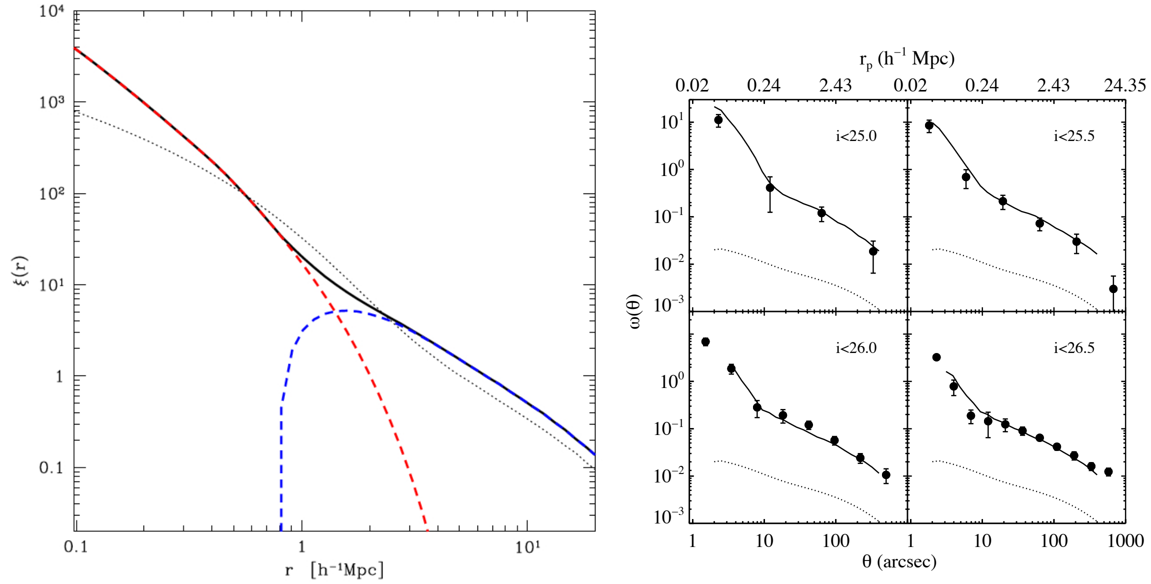

Figure 9.9: *Left:* A prediction for the correlation function $\xi(r)$ from the halo model. The dotted line shows the two-point real-space correlation function for dark matter in a consensus cosmology (Appendix A), while the solid black curve shows the predicted correlation function for a sample of local galaxies with r-band absolute magnitude $M_r < -21.7$. This is the sum of two contributions. The first is from galaxies within the same dark matter halo (the "one-halo term"), reflecting the radial distribution of galaxies within halos, and shown by the red dashed curve. The second contribution comes from the clustering between galaxies in different dark matter halos, reflecting the clustering of the underlying halos; this "two-halo term" will be greater for populations of galaxies found in more massive (and hence more highly biased) dark matter halos. Figure provided by A. Zentner. *Right:* Projected correlation function for galaxies at $z \sim 4$ from the GOODS survey, compared to a model based on abundance matching with dark matter halos and subhalos. The scale of the typical halo hosting the galaxies is clearly seen even in the projected correlations. Figure from Conroy et al. (2006).

grows greater, but decrease as the redshift distribution $\frac{dN}{dz}$ grows wider, as the angular correlations are diluted by projection effects.

If we assume that $\xi(r)$ evolves only slowly with redshift, then for a sample of galaxies with redshift distribution given by a Gaussian centered at z_0 with RMS σ_z (e.g., due to photometric redshift errors or other sample selection effects), the amplitude of w will be proportional to σ_z^{-1}. For the sparsest LSST samples, the error in measuring $w(\theta)$ within some bin will be dominated by Poisson or "shot" noise, leading to an uncertainty $\sigma(w) = (1 + w(\theta))N_p(\theta)^{-1/2}$, where N_p is the number of pairs of objects in the class whose separations would fall in that bin if they were randomly distributed across the sky. This is $N_p = \frac{1}{2}N_{gal}\Sigma_{gal}(2\pi\theta\Delta\theta)$, where N_{gal} is the number of objects in the class of interest, Σ_{gal} is the surface density of that sample on the sky, and $\Delta\theta$ is the width of the bin in θ; since N_p scales as Σ_{gal}^2, $\sigma(w)$ decreases proportional to Σ_{gal}^{-1}.

For large samples or at large scales, the dominant contribution to errors when measuring correlations with standard techniques is associated with the variance of the integral constraint (Peebles 1980). This variance is related to the "cosmic" or sample variance due to the finite size of a field – i.e., it is a consequence of the variation of the mean density from one subvolume of the Universe to another – and is roughly equal to the integral of $w(\theta)$ as measured between all possible pairs of locations within the survey (Bernstein 1994). This error is independent of separation and is highly covariant amongst all angular scales. However, it may be mitigated or eliminated via a suitable choice of correlation estimator (e.g., Padmanabhan et al. 2007). For a 20,000 deg^2 survey with square geometry (the most pessimistic scenario), for a sample with correlation length, r_0, correlation slope, $\gamma = 1.8$, and redshift distribution described by a uniform distribution about $z = 1$ with spread, Δz, the amplitude of $w(\theta)$ will be

$$w = 0.359 \left(\frac{\theta}{1 \text{ arcmin}}\right)^{1-\gamma} \left(\frac{r_0}{4\,h^{-1}\text{Mpc}}\right)^{\gamma} \left(\frac{\Delta z}{0.1}\right)^{-1}, \tag{9.2}$$

while the contribution to errors from the variance of the integral constraint will be approximately (Newman & Matthews, in preparation):

$$\sigma_{w,ic} \approx 5.8 \times 10^{-4} \left(\frac{r_0}{4\,h^{-1}\text{Mpc}}\right)^{\gamma} \left(\frac{\Delta z}{0.1}\right)^{-1}. \tag{9.3}$$

For sparse samples at modest angles, where Poisson noise dominates (or equivalently if we can mitigate the integral constraint variance) if we assume the sample has a surface density of Σ_{gal} objects deg^{-2} over the whole survey, the signal-to-noise ratio for a measurement of the angular correlation function in a bin in angle with width 10% of its mean separation will be

$$S/N = 47.4 \left(\frac{r_0}{4\,h^{-1}\text{Mpc}}\right)^{\gamma} \left(\frac{\Delta z}{0.1}\right)^{-1} \left(\frac{\Sigma_{gal}}{100 \text{ deg}^{-2}}\right) \left(\frac{\theta}{1 \text{ arcmin}}\right)^{2-\gamma}. \tag{9.4}$$

In contrast, for larger samples (i.e., higher Σ_{gal}), for which the variance in the integral constraint dominates, the S/N in measuring w will be nearly independent of sample properties, $\sim 600(\theta/1 \text{ arcmin})^{1-\gamma}$. Thus, even if the variance in the integral constraint is not mitigated, w should be measured with S/N of 25 or better at separations up to $\sim 0.9°$, and with S/N of 5 or better at separations up to $\sim 7°$. The effectiveness of LSST at measuring correlation functions changes slowly with redshift: the prefactor in Equation 9.4 is 91, 55, 50, or 71 for $z = 0.2$, 0.5, 1.5, or 3.

As a consequence, even for samples of relatively rare objects – for instance, quasars (see § 10.3 and Figure 10.10), supernovae, or massive clusters of galaxies – LSST will be able to measure angular correlation functions with exceptional fidelity, thanks to the large area of sky covered and the precision of its photometric redshifts. This will allow detailed investigations of the relationship between dark matter halos and galaxies of all types: the one-halo–two-halo transition (cf. § 9.5.4) will cause $\sim 10\%$ deviations of $w(\theta)$ from a power law at $\sim$ Mpc scales in correlation functions for samples spanning $\Delta z \sim 0.1$ (Blake et al. 2008), which will be detectable at $\sim 5\sigma$ even with highly selected subsamples containing $< 0.1\%$ of all galaxies from LSST. The ensemble of halo models (or parameter-dependent halo models) resulting from measurements of correlation functions for subsets of the LSST sample split by all the different properties described in § 9.2 will allow us to determine the relationship between the nature of galaxies and their environments in unprecedented detail. In the next few years, we plan to develop and test techniques for measuring halo model parameters from angular correlations using simulated LSST data sets, so that we may more precisely predict what can and cannot be measured in this manner.

Measuring the spatial clustering of the dark matter halos hosting galaxies over a wide range of cosmic time will allow us to trace the evolution of galaxy populations from one epoch to another by identifying progenitor/descendant relationships. Equation 9.5.4 shows an example of what LSST will reveal about the clustering of galaxy populations as a function of redshift. Here, "bias" refers to the average fluctuation in number density of a given type of galaxies divided by that of the dark matter particles. The redshift bins were chosen to have width of $\delta_z = 0.05 \times (1+z)$, i.e., somewhat broader than the expected LSST photometric redshift uncertainties. In this illustrative model, high-redshift galaxies discovered by LSST are broken into 100 subsets, with three of those subsets corresponding to the bluest, median, and reddest rest-ultraviolet color plotted. Those three subsets were assumed to have a correlation length evolving as $(1+z)^{0.1}$. Uncertainties were generated by extrapolating results from the 0.25 deg^2 field of Francke et al. (2008), assuming Poisson statistics and a constant observed galaxy number density over $1 < z < 4$ that falls by a factor of ten by $z = 6$ due to the combination of intrinsic luminosity evolution and the LSST imaging depths. In this particular model, the bluest galaxies at $z = 6$ evolve into typical galaxies at $z \sim 2$, and typical galaxies at $z = 6$ evolve into the reddest galaxies at $z \sim 3$. The breakdown into 100 galaxy subsets based on color, luminosity, size, etc. with such high precision represents a tremendous improvement over current observations; the figure illustrates the large error bars that result when breaking current samples into 2–3 bins of color (points labeled C08,A05b) or luminosity (points labelled L06,Ou04).

Higher-order Correlation Functions

Measuring higher-order correlation statistics (such as the three-point function – the excess probability of finding three objects with specified separations from each other – or the bispectrum, its Fourier counterpart) provides additional constraints on the relationship between galaxies and dark matter not available from two-point statistics alone (e.g., Verde et al. 2002, see also § 13.5). Whereas the techniques for measuring two-point statistics (Martínez & Saar 2002) are quite mature, measuring and interpreting higher-order correlation functions is an active field which will evolve both before and during LSST observations. Therefore, although these higher-order correlation functions will be used to constrain the relationship of galaxies to dark matter for broad galaxy samples (e.g., linear, non-linear, or stochastic biasing models, or HOD-based models), we expect that most of the effort in this field in the LSST context will be in the large-scale-structure context, as described in § 13.5, rather than focused specifically on galaxy evolution. The ultimate result of this research will be a calibration of the large-scale structure bias of samples of galaxies observed by LSST, putting relative bias measurements coming from two-point functions on an absolute scale and improving all halo modeling.

Cross-correlations

As described above, the auto-correlation function – which measures the clustering of objects in some class with other objects of the same type – can provide information about the relationship of those objects to the underlying hierarchy of large-scale structure. A related quantity, the angular two-point, cross-correlation function (the excess probability over Poisson of finding an object of one type near an object of a second type, measured as a function of separation) is a sensitive probe of the underlying relationships between any two different classes of extragalactic objects.

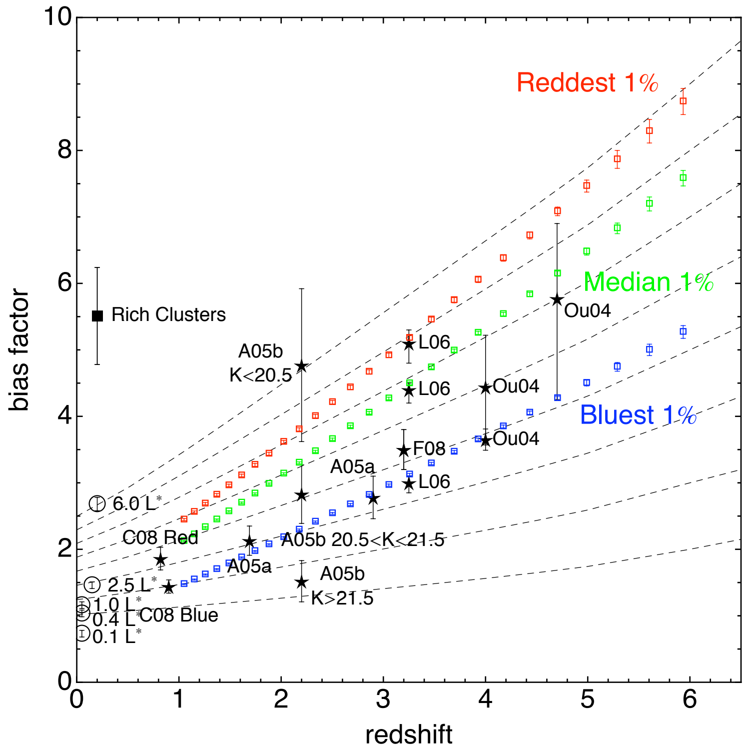

Figure 9.10: Evolution of galaxy bias versus redshift for three LSST galaxy samples at $1 < z < 6$. The three samples are selected to be the 1% of all LSST galaxies at each redshift that is the bluest/median/reddest in rest-ultraviolet color. The dashed evolutionary tracks show the evolution in bias factor versus redshift based on the Sheth-Tormen conditional mass function. Points with error bars show a compilation of literature bias values for $z = 1.7$ color-selected galaxies (A05a, Adelberger et al. 2005b), $z = 2.1$ color selected galaxies (A05b, Adelberger et al. 2005a), $z \sim 3$ Lyman break galaxies (A05a; F08, Francke et al. 2008; L06, Lee et al. 2006), and $z > 4$ Lyman break galaxies (Ou04, Ouchi et al. 2004). Also shown are $z \sim 1$ galaxies separated by color (C08, Coil et al. 2008), $z \sim 0$ galaxies labeled by their optical luminosity, from Zehavi et al. (2005) and rich galaxy clusters from Bahcall et al. (2003).

As an example, the clustering of galaxies of some type (e.g., blue, star-forming galaxies) around cluster centers provides a measurement of both the fraction of those galaxies that are associated with clusters, and their average radial distribution within a cluster. Hence, even though with photometric redshifts we *cannot* establish whether any *individual* galaxy belongs to one particular cluster, we *can* determine with high precision the *average* galactic populations of clusters of a given sort (mass, richness, and so on).

Cross-correlation functions are particularly valuable for studying rare populations of objects for which they may be measured with much higher S/N than auto-correlations. The amplitude of the angular correlation function between two classes, A and B, with redshift distributions, dN_A/dz and dN_B/dz, is:

$$w_{AB}(\theta) = \frac{\int dz \, \frac{dN_A}{dz} \int dz' \, \xi_{AB}(r\theta, z') \, \frac{dN_B}{dz'}}{\left(\int dz' \, \frac{dN_A}{dz'}\right) \left(\int dz \, \frac{dN_B}{dz}\right)}. \tag{9.5}$$

In the weak-clustering regime, which will generally be applicable for LSST samples at small scales, the error in $w_{AB}(\theta)$ will be $(1+w_{AA})^{1/2}(1+w_{BB})^{1/2}N_{AB}(\theta)^{-1/2}$, where w_{AA} is the auto-correlation of sample A, w_{BB} is the auto-correlation of sample B, and N_{AB} is the number of pairs of objects in each class separated by θ, if the samples were randomly distributed across the sky.

In the limit that the redshift distributions of samples A and B are identical (e.g., because photometric redshift errors are comparable for each sample), the auto-correlations and cross-correlations of samples A and B have the familiar power law scalings, the S/N for measuring w_{AB} will be larger than that of w_{AA} on large scales by a factor of $(r_{0,AB}/r_{0,AA})^{\gamma}(\Sigma_B/\Sigma_A)^{1/2}$, where Σ_A and Σ_B are the surface densities of samples A and B on the sky and $r_{0,AB}$ and $r_{0,AA}$ are the scale lengths for the cross-correlation and auto-correlation functions.

Cross-correlations as a Tool for Studying Galaxy Environments

It would be particularly desirable to measure the clustering of galaxies of a given type with the underlying network of dark matter. One way of addressing this is measuring the lensing of background galaxies by objects in the class of interest (§ 14.2); this is not possible for rare objects, however. An alternative is to determine the cross-correlation between objects in some class of interest with all galaxies at a given redshift ("tracers"). This function, integrated to some maximum separation r_{max}, will be proportional to the average overdensity of galaxies within that separation of a randomly selected object. For linear biasing, this quantity is equal to the bias of the tracer galaxy sample times the overdensity of dark matter, so it is trivial to calculate the underlying overdensity. The mapping is more complicated if biasing is not linear; however, the exquisitely sensitive correlation function measurements that LSST will provide will permit halo modeling of nonlinear bias allowing accurate reconstruction.

This measurement is essentially equivalent to the average overdensity measured from large-scale galaxy environment studies (Blanton & Berlind 2007; Blanton et al. 2005; Cooper et al. 2008); an advantage is that clustering measurements can straightforwardly probe these correlations as a function of scale. With LSST, such comparisons will be possible for even small samples, establishing the relationship between a galaxy's multivariate properties and the large-scale structure environment where it is found; see Figure 9.11 for an example of the utility of cross-correlation techniques.

The cross-correlation of two samples is related to their auto-correlation functions by factors involving both their relative bias and the stochastic term (Dekel & Lahav 1999), thus one can learn something about the extent that linear deterministic bias holds for the two samples (Swanson et al. 2008). As another example, associating blue, star forming galaxies with individual galaxy clusters will be fraught with difficulties given photometric redshift errors, but the cluster-blue galaxy cross-correlation function will determine both the fraction of blue galaxies that are associated with clusters and also their average radial distribution within their host clusters (see Coil et al. 2006 for an application with spectroscopic samples). This will allow us to explore critical questions such as what has caused the strong decrease in galaxies' star formation rates since $z \sim 1$, what mechanism suppresses star formation in early-type galaxies, and so on.

AGN may provide one critical piece of this puzzle; feedback from AGN can influence the cooling of gas both on the scale of galaxies and within clusters (Croton et al. 2006; Hopkins et al. 2008) and the black-hole mass/bulge-mass correlation strongly suggests that black hole growth and galaxy growth go hand-in-hand. By measuring the cross-correlation of AGN (e.g., selected by variability) with galaxies (as a function of their star formation rate, for instance) and with clusters, we can test detailed scenarios for these processes. See the discussion in § 10.3. The evolution of low-mass galaxies within larger halos could also be influenced by tides, mergers, gas heating and ionization from nearby galaxies, and other effects; mapping out the types of galaxies found as a function of cluster mass and clustocentric distance can constrain which of these phenomena is most important.

Cross-correlation against LSST samples will also boost the utility of a variety of future, complementary multi-wavelength data sets. Even unidentified classes of objects found at other wavelengths (e.g., sub-millimeter sources, sources with extreme X-ray to optical brightness ratios, etc.) may be localized in redshift and their dark matter context identified by measuring their correlation with galaxies or structures of different types and at different redshifts; cross-correlations will be strong only when objects of similar redshift and halo mass are used in the correlation. In this way, LSST data will be a vital tool for understanding data sets which may be obtained long after the survey's completion.

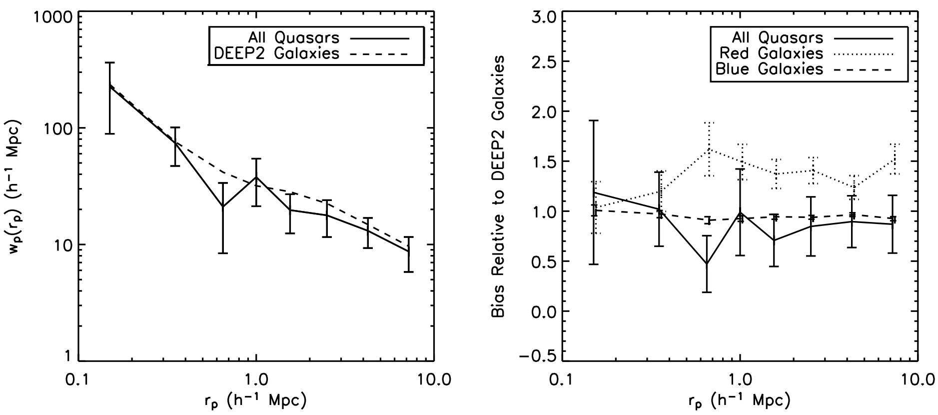

Figure 9.11: A demonstration of the power of cross-correlation techniques for rare samples, from Coil et al. (2007). The left panel shows the projected two-point cross-correlation between a sample of only 52 quasars at $0.7 < z < 1.4$ identified using spectroscopy from the SDSS or the DEEP2 Galaxy Redshift Survey, and a comparison sample of ~ 5000 DEEP2 galaxies. The dashed curve indicates the auto-correlation of the comparison galaxy sample. From these measurements, Coil et al. determined the relative bias of quasars to the DEEP2 galaxy sample, and with similar techniques measure the relative bias of blue or red galaxies within DEEP2 to the overall sample, as shown in the right panel. See Figure 10.10 for predicted errors for LSST data.

Cross-correlations as a Tool for Studying Galaxy Dust

Another application of cross-correlation techniques is to measure properties of the dust content of dark matter halos and the intergalactic medium. For a given redshift slice of galaxies, the light from galaxies behind the sample has to travel through the dust associated with the foreground galaxies. Ménard et al. (2009b) show that the dust halos surrounding field galaxies in the SDSS generates a detectable reddening in the colors of background quasars. By cross-correlating quasar colors (rather than the positions of quasars) with foreground galaxy density, Ménard et al. (2009b) were able to detect dust halos extending well beyond $100h^{-1}$kpc for typical $0.5L^*$ galaxies. This, in turn, leads to an opacity of the Universe which is a potential source of systematic bias for planned supernova surveys (Ménard et al. 2009a).

With LSST, we will be able to extend these measurements in a number of ways. Of particular interest is looking at the evolution of these dust halos as a function of redshift. With the relatively shallow depth of the SDSS data (and the need for high foreground and background object density on the sky to detect the signal), measurements with current data will be limited to redshifts below $z \sim 0.5$. With the much greater depth available in LSST, these limits should be doubled at the least, perhaps even taken as high as $z \sim 2$, depending on the efficiency of finding r and i band drop-out galaxies. Going to higher redshifts will mean a stronger signal as the rest-frame wavelength of the background sample light shifts to the ultraviolet where extinction should be stronger. More importantly, however, this shift into the UV will break a number of degeneracies in the current measurements, which are unable to distinguish between Milky Way or LMC-like extinction curves. This, in turn, would tell us if the bulk of the dust was more silica or graphite-based (Draine & Lee 1984) and offer clues as to how these extended dust halos may have formed.

9.6 Galaxies at Extremely Low Surface Brightness

As the deepest wide-field optical survey currently planned, LSST will push observations of galaxies to lower surface brightness than has ever been available over such a large field. This capability will allow a better understanding of the outskirts of galaxies, of the merger history of galaxies, of the role of tidal stripping in groups and clusters, and of the lowest surface brightness dwarfs and their evolution. In § 7.9, we discussed the discovery of nearby examples of extremely faint galaxies in resolved stars; here we do so in diffuse light. To push LSST data to its faintest limits will require a dedicated analysis effort; as found in SDSS, detection, deblending, and photometry at low surface brightness levels requires a different analysis than that necessary for stellar photometry. For example, while the formal signal-to-noise ratio of the data will be sufficient to detect signal at less than 1/1000 the sky level on scales of many arcseconds, clearly to really achieve that precision requires an exquisite understanding of scattered light and other systematics, to distinguish true galaxies with, for example, ghosts from bright stars, variations in the background sky, and other artifacts.

9.6.1 Spiral Galaxies with Low Surface Brightness Disks

Low surface brightness (LSB) spirals are diffuse galaxies with disk central surface brightness fainter than 22.5 mag arcsec^{-2} in the B band. They are generally of quite low metallicity, and thus exhibit little dust or molecular gas, but have quite large neutral hydrogen content (O'Neil et al. 2000a,b, 2003; Galaz et al. 2002, 2006, 2008) and star formation rates lower than 1 $M_\odot$ yr^{-1} (Vallenari et al. 2005). Rotation curves of LSBs extend to large radii (de Blok & Bosma 2002), and, therefore, their dynamics are dark matter dominated. Several studies have shown that LSBs dominate the volume density of galaxies in the Universe (e.g., Dalcanton et al. 1997), and thus it is of prime importance to understand them in the context of the formation of spiral galaxies.

Given the depth and scattered light control that LSST will have (§ 3.4), it should be sensitive to galaxies with central surface brightness as low as 27 mag arcsec^{-2} in r in the ten-year stack –

compared with SDSS, where the faintest galaxies measured have $\mu_r \sim 24.5$ mag arcsec^{-2} (Zhong et al. 2008). Scaling from the estimates of LSB surface density from Dalcanton et al. (1997), we conservatively estimate that LSST will discover 10^5 objects with $\mu_0 > 23$ mag arcsec^{-2}. Indeed, this estimate is quite uncertain given our lack of knowledge of the LSB population demographics. LSST's combination of depth and sky coverage will allow us to settle at last the contribution of very low surface brightness galaxies to the volume density of galaxies in the Universe.

LSST will also discover large numbers of giant LSB spirals, of which only a few, such as Malin 1 (Impey & Bothun 1989), are known, and tie down the population of red spiral LSBs. ALMA will be ideal for studying the molecular content and star formation of these objects.

9.6.2 Dwarf Galaxies

The other prominent members of the LSB world are dwarf galaxies. Low luminosity galaxies are the most numerous galaxies in the Universe, and are interesting objects for several reasons. They tend to have had the least star formation per unit mass of any systems, making them interestingly pristine tests of small-scale cosmology. For the same reason, they are important testbeds for galaxy formation: Why is their star formation so inefficient? Does the molecular cloud model of star formation break down in these systems? Do outflows get driven from such galaxies? Does reionization photo-evaporate gas in the smallest dwarfs? However, dwarf galaxies also tend to be the galaxies of lowest surface brightness. For this reason, discovery of the faintest known galaxies has been limited to the Local Group, where they can be detected in resolved stellar counts (§ 7.9). Here we discuss the discovery of such objects in diffuse light at larger distances.

We know that for larger galaxies, the effects of environment are substantial — red galaxies are preferentially foud in dense environments. Thus, we need to study dwarfs in environments beyond the Local Group. Questions about the importance of reionization relative to ram pressure and tidal stripping hinge crucially on the field dwarf population — and extremely deep, wide-field surveys are the only way to find these galaxies, especially if reionization has removed their gas.

Based on the early-type galaxy luminosity function of Croton et al. (2005), with a faint-end slope $\alpha = -0.65$, we can expect $\sim 2 \times 10^5$ early-type dwarfs brighter than $M_V = -14$ within 64 Mpc. Figure 9.6 and Figure 9.7 suggest that such galaxies will be relatively easy to find within this distance. Pushing to lower luminosities, the same luminosity function predicts 8×10^3 dwarf spheroidal galaxies at $D < 10$ Mpc brighter than $M_V = -10$. However, we have no business extrapolating this luminosity function to such low luminosities. Using the same M^* and ϕ^*, but changing the slope to $\alpha = -1$, changes the prediction to 2.5×10^5 galaxies. Clearly, probing to such low luminosities over large areas of the sky will provide a lot of leverage for determining the true faint end slope and its dependence on environment.

Spectroscopy may not be the most efficient way to confirm that these are actually nearby dwarf galaxies (Figure 9.7). At $M_V = -10$, the surface brightnesses are generally too low for most spectrographs. However, many will be well enough resolved to measure surface-brightness fluctuations (Figure 9.12). Followup observations with HST, JWST, or JDEM can resolve the nearby galaxies into individual stars, confirming their identification and measuring distances from the tip of the red-giant branch.

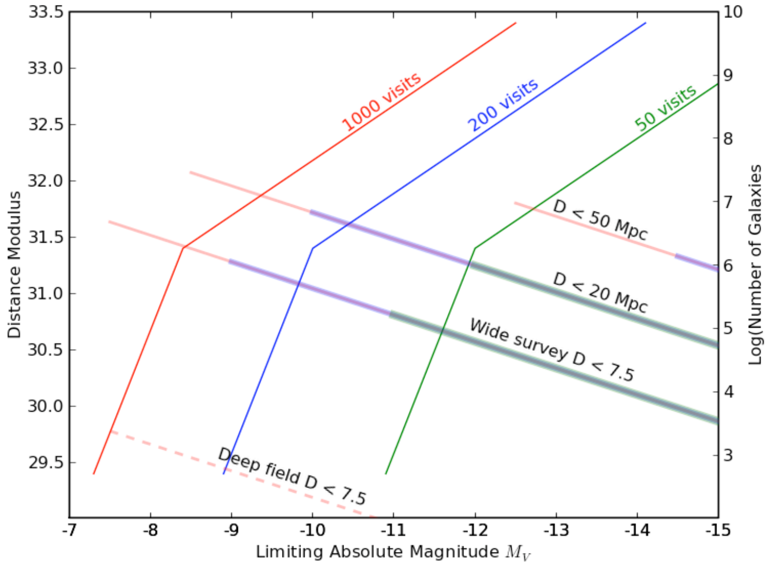

Figure 9.12: LSST surface brightness fluctuations, whereby mottling of the galaxy image due to the finite number of stars in each pixel is a measure of the distance to the galaxy. The curves moving upwards to the right show distance modulus vs. absolute magnitude for distance modulus determination to a precision of 0.5 mag for 50, 200, and 1,000 r-band visits (the latter appropriate to the deep drilling fields). This is derived by scaling from the realistic image simulations of Mieske et al. (2003), which include the effects of photon statistics, resolution, and image size. The curves moving upwards to the left show the expected number of galaxies in a 20,000 deg^2 survey (solid lines) or a 10 deg^2 deep-drilling field with 1,000 visits (dashed line near the bottom). Numbers are based on the luminosity function of Croton et al. (2005).

9.6.3 Tidal Tails and Streams

One of the major recent advances in astronomy has been the discovery of ubiquitous tidal streams of disrupted dwarf galaxies surrounding the Milky Way and other nearby galaxies (§ 7.6). The existence of such streams fits well into the hierarchical picture of galaxy formation, and has caused a re-assessment of traditional views about the formation and evolution of the halo, bulge, and disk of our Galaxy.

The streams can be studied in detail through resolved stars, but only a few galaxies are close enough to be studied in this way. Studies of more distant galaxies in diffuse light will be important for understanding the demographics of streams in general. Such studies have a bearing on a variety of interesting issues. The streams are heated by interaction with dark matter sub-halos within the larger galaxy halo. Statistical studies of the widths of tidal streams may thus provide some constraints on the clumpiness of dark matter halos. This is important because ΛCDM models predict hundreds of dwarf galaxy mass halos in Milky Way size galaxies, whereas we only know of a few dozen such galaxies. This could be telling us that the dark matter power spectrum cuts off at dwarf galaxy scales, or it could be signaling that star formation is suppressed in low-mass halos. The shapes of tidal streams also provide constraints on the shapes of galaxy halos. This can be studied statistically using large samples of tidal streams revealed by deep images (e.g. Figure 9.13, Figure 9.14). By the time LSST begins observing, we expect that hundreds of individual galaxies will have been targeted for deep study with other facilities. LSST, however, will allow us to create a deep, unbiased statistical survey of thousands more galaxies.

Figure 9.13: Low surface brightness tidal streams surrounding NGC5907. This is a $>$ 10 hr exposure taken on a 0.5-meter telescope; the faintest features apparent have a surface brightness below 28 mag arcsec^{-2} in r. From Martínez-Delgado et al. (2008).

At $z = 0.1$, a semi-major axis of 50 kpc corresponds to $27''$. A dwarf galaxy of absolute magnitude $M_{R,AB} = -16$ stretched uniformly around a circular stream of radius $27''$ with a half-light width of 2 kpc will have a mean surface brightness of $\mu_{R,AB} = 29.2$, 0.07% the mean dark-sky brightness. The ability to detect and measure the parameters of such streams depends critically on the flatness of the LSST sky background or the ability to model it.

9.6.4 Intracluster Light

Moving from individual galaxies to groups and clusters, we expect the tidal streams that existed during the early stages of galaxy formation to have been smoothed out into a diffuse stellar halo interspersed between the galaxies. Purcell et al. (2007) calculate that the fraction of the total stellar mass in this intra-halo population should range from $\sim$ 8% to $\sim$ 20% for halo masses ranging from 10^{13} to $10^{15} M_{\odot}$; these numbers are roughly confirmed in the deep imaging study of the Virgo cluster by Mihos et al. (2005). The uniformity of the LSST data should enable careful measurements of this diffuse light with very large samples of nearby groups and clusters, to probe both the trend with group mass and the trends with other properties of the groups. Stacking large

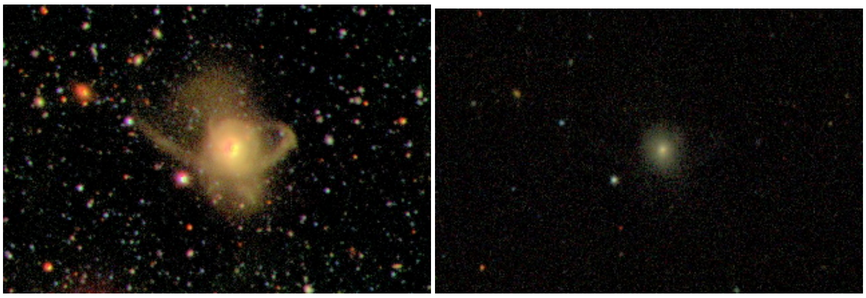

Figure 9.14: *Left:* MUSYC UVR image of a $z = 0.1$ galaxy with red low surface brightness features revealing a recent interaction without active star formation (van Dokkum 2005). This image reaches a 1σ surface brightness limit of mag 29.5 arcsec^{-2}, a good match to the expected LSST depth. *Right:* SDSS gri image of the same $3' \times 2'$ piece of sky, showing that these features are not accessible to the current generation of full-sky surveys beyond the very local Universe.

numbers of groups after masking the galaxies will enable the mean halo light profile to be traced to very low surface brightness.

Novae will provide a unique way to probe diffuse light. Shara (2006) estimates that LSST will obtain good light curves and hence distance estimates for ~ 50 *tramp* novae per year within 40 Mpc if the diffuse stellar mass is 10% of the stellar mass in galaxies. We might consider putting one of the LSST deep drilling fields (§ 2.1) on a nearby cluster of galaxies such as Fornax. If 10% of the total stellar mass of Fornax ($\sim 2.3 \times 10^{11} M_\odot$) in intracluster light, and we observed it 9 months of every year, we would discover roughly 170 intra-cluster novae.

9.7 Wide Area, Multiband Searches for High-Redshift Galaxies

Deep, narrow surveys with space-borne telescopes have identified new populations of high-redshift galaxies at redshifts $z > 5$ through photometric dropout techniques. While these observational efforts have revolutionized our view of the high-redshift Universe, the small fields of such surveys severely limit their constraining power for understanding the bright end of the high-redshift galaxy luminosity function and for identifying other rare objects, including the most massive, oldest, and dustiest galaxies at each epoch. By combining the power of multi-band photometry for dropout selection and the unprecedented combination of wide area and deep imaging, LSST will uncover the rarest high-redshift galaxies (Figure 9.5). The discovery and characterization of the most massive galaxies at high redshift will provide new constraints on early hierarchical structure formation and will reveal the galaxy formation process associated with high-redshift quasars (§ 10.1.1).

Observations of i-dropout and z-dropout galaxies in the Hubble Ultra Deep and GOODS fields have enabled a determination of the rest-UV luminosity function of $z \sim 6$ galaxies (e.g., Dickinson et al. 2004; Bunker et al. 2004; Yan & Windhorst 2004; Malhotra et al. 2005; Yan et al. 2006; Bouwens et al. 2004, 2006). There is a scatter of 1-2 orders of magnitude in determinations of the bright end of the LF. Figure 9.15 shows the galaxy source count surface densities for $5.5 \lesssim z \lesssim 7$ galaxies in the z-band calculated from a range of $z \sim 6$ rest-frame UV luminosity functions taken from the literature. LSST will increase the counts of galaxy candidates at $z > 5.5$ by ~ 5 orders of magnitude. The LSST survey will probe almost the entire luminosity range in this figure and

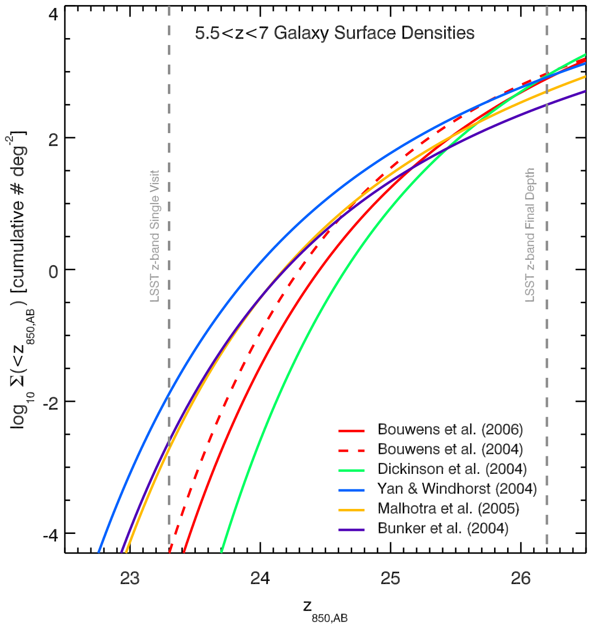

Figure 9.15: Fits to measured galaxy source count surface densities for $5.5 \lesssim z \lesssim 7$ galaxies in the z-band, as measured by different surveys. Note the tremendous variation, especially at the bright end, caused by the small areas that these surveys cover.

should find hundreds of $z_{850} \sim 23 - 24$ galaxies at $z \sim 6$. The resulting uncertainty on their abundance will be a few percent, 2–3 orders of magnitude better than currently available.

Observatories such as JWST will reach extremely deep sensitivities, but it cannot survey large areas of sky; for example, the Deep Wide Survey discussed in Gardner et al. (2006) will be only $\sim$100 arcmin^2. For extremely rare objects such as luminous high-redshift galaxies, JWST will rely on wide-area survey telescopes such as LSST for follow-up observations. Wide-area surveys of the far infrared, submillimeter, and millimeter sky may also be capable of finding rare, massive galaxies at high-redshift through dust emission powered by star formation or AGN activity. The Herschel-ATLAS survey[1] will survey 550 deg^2 at $110 - 500\mu$m down to sensitivities of < 100 mJy. The SCUBA-2 “All-Sky” Survey[2] will map the entire 850μm sky available to the James Clerk Maxwell Telescope to 30 mJy/beam. The South Pole Telescope (Carlstrom et al. 2009) will detect dusty galaxies over 4000 deg^2 at $90 - 270$ GHz to a $1\,\sigma$ sensitivity of 1 mJy at 150 GHz. Surveys such as these will complement the LSST wide area optical survey by providing star formation rate and bolometric luminosity estimates for rare, high-redshift galaxies.

A primary goal for studying rare, high-redshift galaxies will be to understand the galaxy formation process associated with luminous quasars at $z = 5 - 6$ with supermassive black holes (SMBHs) of mass $> 10^9\,M_\odot$. This problem, first popularized by Efstathiou & Rees (1988), involves finding a robust way of growing SMBHs quickly in the limited time available before $z \sim 6$. Recent work simulating the formation of a $z \sim 6$ quasar with a SMBH mass of $\sim 10^9$ M$_\odot$ (Li et al. 2007) has provided a theoretical argument that high-redshift quasars can be explained naturally in the

[1] http://h-atlas.astro.cf.ac.uk/science/h-atlas_final_proposal.pdf
[2] http://www.jach.hawaii.edu/JCMT/surveys/sassy/

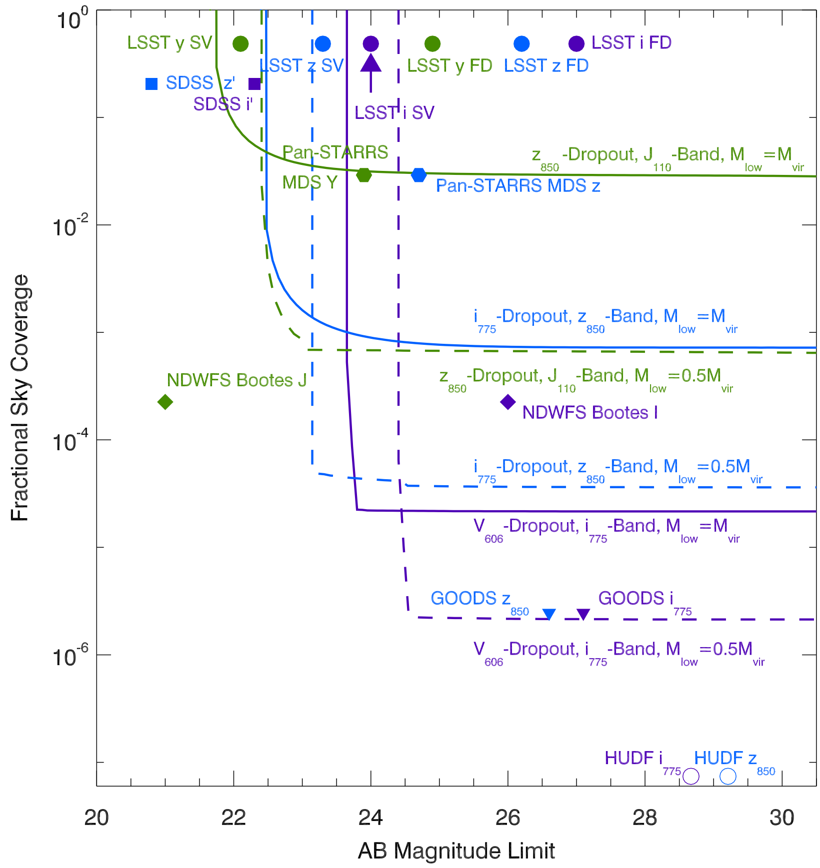

Figure 9.16: Estimated survey parameters required to find $z \gtrsim 7$ quasar progenitors and quasar descendants at redshifts $7 \gtrsim z \gtrsim 4$. Shown is the fractional sky coverage and AB magnitude limit needed to build V_{606}-dropout (purple), i_{775}-dropout (blue), and z_{850}-dropout (green) samples that include a galaxy more massive than the virial mass $M_{\rm vir}$ (solid line) or $0.5M_{\rm vir}$ (dashed line) of the simulated $z \sim 6$ quasar host from Li et al. (2007). As the dropout selection moves to redder bands and higher redshifts, the co-moving volume and redshift interval over which massive galaxies satisfy the selection criteria decreases. The co-moving number density of massive galaxies, calculated using the Sheth & Tormen (1999) mass function, also declines rapidly at high redshifts. The combination of these effects requires large fractional sky coverage to find starbursting quasar progenitors at $z \gtrsim 7$. The circles show the parameters of the existing Hubble UDF (i_{775}- and z_{850}-bands, open circles), GOODS (i_{775}- and z_{850}-bands, triangles), SDSS (i- and z-bands, squares), and NOAO Wide Deep Field Survey (I- and J-bands, diamonds) observations. Future wide area surveys with red sensitivity, such as LSST (i, z, and y Single Visit and Final Depths, solid circles), or possibly the Pan-STARRS Medium Deep Survey (z- and Y-band, hexagons), could find quasar progenitors at $z \gtrsim 6$ if their two reddest bands reach $\gtrsim 22$ AB magnitude sensitivity. Adapted from Robertson et al. (2007).

context of the formation of galaxies in rare density peaks in the ΛCDM cosmology. A clear test of this picture is the predicted population of very rare, massive starburst galaxies at redshifts $z > 5$. Robertson et al. (2007) performed a detailed characterization of the observable ramifications of this scenario, the foremost being the possible detection of the starbursting progenitors of $z \sim 4-6$ quasars with massive stellar populations ($M_* \sim 10^{11-12}\,M_\odot$) at higher redshifts in wide area, Lyman-break dropout samples. Such objects should be very strongly clustered, as is found for high-redshift quasars (Shen et al. 2007; see the discussion in § 10.3).

Figure 9.16 shows the area and depth required for a photometric survey to identify the high-redshift progenitors of $z \sim 4-6$ quasars. To find a single such galaxy in i-dropout and z-dropout samples at $z > 5$ and $z > 6$, a survey must cover $> 5\%$ of the sky with a depth of $z_{AB} \sim 23-24$ and $y \sim 21.7-22.5$, respectively. These requirements are remarkably well-matched to the single visit LSST limiting magnitudes ($z_{AB} \sim 23.3$, $y \sim 22.1$, see Figure 9.5). Given that these requirements are unlikely to be realized by surveys before LSST, the identification of rare high-redshift galaxies could provide an exciting early LSST science discovery. With the substantially deeper co-added depth of the repeated LSST visits, the sample of rare, high-redshift galaxies would increase rapidly.

9.8 Deep Drilling Fields

The currently planned LSST cadence (§ 2.1) involves ∼10 pointings on the sky that will be observed more frequently, with a cadence and filter distribution that can be optimized for finding e.g., supernovae. Significantly enhanced science can be achieved by spending proportionally more time in *uzy* than *gri* in order to achieve more equal depth in the six filters. By switching to a fractional observing time distribution of 9, 1, 2, 9, 40, 39 % in *ugrizy* respectively, and 1% of total the LSST observing time on each drilling field, we would achieve $5\,\sigma$ point source detection depths of 28.0, 28.0, 28.0, 28.0, 28.0, and 26.8 respectively[3]. This is shown by the triangles in Figure 9.5. This would also avoid hitting the confusion depth at g and r of ∼ 29 mag.

These deep drilling fields present a number of opportunities for coordinated deep multiwavelength imaging to select targets for narrow field follow-up with JWST, ALMA, and other facilities. Deep infrared coverage is critical for photometric redshifts. Ideal field locations for extragalactic work are those at high Galactic latitude with minimal dust extinction. There are several existing fields with wide-deep multiwavelength coverage that represent likely locations for LSST Deep Fields, e.g., the Extended Chandra Deep Field-South, COSMOS/Ultravista, the equatorial complex of Subaru-XMM Deep Survey/Deep2 Field 4/VVDS 0226-0430/CFHT LS D1/XMM-LSS/NDWFS Cetus/UKIDDS UDS/SpUDS, VISTA VIDEO fields, and the Akari Deep Field-South. None of these yet covers a full LSST field of view at the desired depth for complementary wavelengths, but once the LSST Deep Field locations are declared, the international astronomy community will be encouraged to conduct wide-deep surveys with near-infrared (VISTA, NEWFIRM), mid-infrared (warm Spitzer), far-infrared (Herschel), ultraviolet (GALEX), sub-millimeter (APEX, ASTE, LMT), and radio (EVLA, SKA) telescopes on these locations.

These multiwavelength concentrations will be natural locations for extensive spectroscopic follow-up, yielding three-dimensional probes of large-scale structure and allowing the calibration of LSST-

[3]The detection limit for resolved galaxies will be brighter than that for point sources.

only photometric redshifts for use elsewhere on the sky. They will enable a nearly complete census of baryonic matter out to $z \sim 7$ traced via the star formation rate density (rest-ultraviolet plus far-infrared to get the total energy from stars), stellar mass density, and gas mass density as a function of redshift. Thus LSST will move us towards a complete picture of galaxy formation and evolution.

9.9 Galaxy Mergers and Merger Rates

Galaxies must grow with time through both discrete galaxy mergers and smooth gas accretion. When and how this growth occurs remains an outstanding observational question. The smooth accretion of gas and dark matter onto distant galaxies is extremely challenging to observe, and complex baryonic physics makes it difficult to infer a galaxy's past assembly history. In contrast, counting galaxy mergers is relatively straightforward. By comparing the frequency of galaxy mergers to the mass growth in galaxies, one can place robust constraints on the importance of discrete galaxy mergers in galaxy assembly throughout cosmic time. The mass accretion rate via mergers is likely to be be a strong function of galaxy mass, merger ratio, environment, and redshift (Stewart et al. 2009); these dependencies can test both the cosmological model and the galaxy-halo connection.

In addition to contributing to the overall buildup of galaxy mass, the violent processes associated with mergers are expected to significantly influence the star formation histories, structures, and central black hole growth of galaxies. However, other physical mechanisms may influence galaxy evolution in similar ways, so direct observations of galaxy mergers are needed to answer the following questions:

• What fraction of the global star formation density is driven by mergers and interactions? Is the frequency of galaxy mergers consistent with the "tightness" of the star formation per unit mass vs. stellar mass relation throughout cosmic time?

• Are typical red spheroids and bulges formed by major mergers, or by secular evolution? Do $z > 1$ compact galaxies grow in size by (minor) mergers?

• Are today's most massive ellipticals formed via dissipationless mergers? If so, when?

• Do gas-rich mergers fuel active galactic nuclei? Which forms first, the bulge or super massive black hole?

In a ΛCDM model, the rate at which dark matter halos merge is one of the fundamental processes in structure formation. Numerical simulations predict that this rate evolves with redshift as $(1+z)^m$, with $1.0 < m < 3.5$ (Gottlöber et al. 2001; Berrier et al. 2006; Fakhouri & Ma 2008; Stewart et al. 2009). It is difficult to directly compare the predicted dark matter halo merger rate with the observed galaxy merger rate due to the uncertainty in the halo occupation number. However, if this comparison is done self-consistently, measuring the merger frequency as a function of cosmic epoch can place powerful constraints on models of structure formation in the Universe.

Numerous observational studies over the past two decades have focused on measuring the galaxy merger rate, yielding highly discrepant values of m, ranging from no evolution ($m \sim 0$) to strong evolution ($m \sim 5$) (Zepf & Koo 1989; Carlberg et al. 1994, 2000; Patton et al. 2000, 2002; Bundy et al. 2004; Lin et al. 2004; Bridge & Carlberg 2007; Lotz et al. 2008a). As a consequence, the importance of galaxy mergers to galaxy assembly, star formation, bulge formation, and supermassive black hole growth is strongly debated. These observational discrepancies may stem from small sample sizes, improperly accounting for the timescales over which different techniques are sensitive, and the difficulty in tying together surveys at high and low redshift with different selection biases.

The galaxy merger rate is traditionally estimated by measuring the frequency of galaxies residing in close pairs, or those with morphological distortions associated with interactions (e.g., double nuclei, tidal tails, stellar bridges). The detection of distortions is done either by visual analysis and classification (Le Fèvre et al. 2000; Bridge et al. 2009 in preparation) or through the use of quantitative measures (Abraham et al. 1996; Conselice 2003; Lotz et al. 2008b). A key uncertainty in calculating the galaxy merger rate is the timescale associated with identifying a galaxy merger. The merger of two comparable mass galaxies may take 1–2 Gyr to complete, but the appearance of the merger changes with the merger stage, thus a given merger indicator (i.e., a close companion or double nucleus) may only be apparent for a fraction of this time (Lotz et al. 2008b). Galaxies at $z < 1$ with clear signatures of merger activity are relatively rare (<10-15% of $\sim$ L* galaxies at $z < 1$, <5% at $z = 0$), although the fraction of galaxies which could be considered to be 'merging' may be significantly higher.

No single study conducted so far has been able to uniformly map the galaxy merger rate from $z = 0$ to $z \geq 2$, as current studies must trade off between depth and volume. An additional limiting factor is the observed wavelength range, as galaxy morphology and pair luminosity ratios are often a strong function of rest-frame wavelength. Very few merger studies have been done with SDSS (optimized for the $z < 0.2$ Universe). SDSS fiber collisions and low precision photometric redshifts prevent accurate pair studies, while the the relatively shallow imaging and moderate ($\sim 1.4''$) seeing reduce the sensitivity to morphological distortions. Deeper spectroscopic and imaging studies probe the $z \sim 0.2 - 1$ Universe, but do not have the volume to also constrain the low redshift Universe or the depth at near-infrared (rest-frame optical) wavelengths to constrain the $z > 1$ Universe. Ultra-deep Hubble Space Telescope studies (GOODS, UDF) can detect L^* mergers at $z > 1$, but have very small volumes and are subject to strong cosmic variance effects. The CFHTLS-Deep survey is well matched to the proposed LSST depths, wavelengths, and spatial resolution, but, with an area 5000 times smaller, is also subject to cosmic variance (Bridge et al., 2009, in preparation).

Unlike the current studies, LSST has the depth, volume, and wavelength coverage needed to perform a uniform study of L^* mergers out to $z \sim 2$, and a statistical study of bright galaxy mergers out to $z \sim 5$. The wide area coverage of LSST will be critical for addressing the effects of cosmic variance on measures of the merger rate, which can vary by a factor of two or more even on projected scales of a square degree (Bridge et al., 2009, in preparation). A variety of approaches will be used to identify mergers in the LSST data:

- Short-lived strong morphological disturbances, such as strong asymmetries and double nuclei, which occur during the close encounter and final merger stages and are apparent for only a few 100 Myr. These will be most easily found in $z \lesssim 0.2$ galaxies, where the LSST $0.7''$ spatial resolution corresponds to 1–2 kpc. Lopsidedness in galaxy surface brightness profiles can provide statistical constraints on minor mergers and requires similar spatial resolution.

- Longer-lived but lower surface brightness extended tidal tails, which occur for ~ 0.5 Gyr after the initial encounter and for up to 1 Gyr after the merger event. These tails are the longest-lived merger signatures for disk-galaxy major mergers, and should be easily detected at $z \leq 1$ in the full depth LSST $r\,i\,z$ images (Figure 9.17 and Figure 9.14). Scaling from the CFHTLS-Deep survey, LSST should detect on the order of 15 million galaxies undergoing a strong tidal interaction.
- Residual fine structures (faint asymmetries, shells, and dust features) detected in smooth-model subtracted images. These post-merger residual structures are visible for both gas-rich and gas-poor merger remnants, and contribute < 1–5% of the total galaxy light, with surface brightnesses ~ 28 mag arcsec^{-2}.
- The statistical excess of galaxy pairs with projected separations small enough to give a high probability for merging within a few hundred Myr. With $\sim 0.7''$ seeing, galaxies with projected separations > 10 kpc will be detectable to $z \sim 5$. LSST's six-band photometry will result in photometric redshift accuracies of about $0.03(1+z)$ (§ 3.8). This is comparable to or better than those used in other studies for the identification of close galaxy pairs, and will allow for the selection of merging galaxies with a wide range in color. With LSST's high quality photometric redshifts and large number statistics, it will be possible to accurately measure the galaxy pair fraction to high precision (although the identification of any given pair will be uncertain). Current surveys detect only about 50-70 red galaxy pairs per square degree for $0.1 < z < 1.0$. With LSST, we should be able to observe more than a million "dry" mergers out to $z \sim 1.0$.

One of the advantages of the LSST survey for studying the evolving merger rate is the dense sampling of parameter space. A large number of merger parameters — galaxy masses and mass ratio, gas fractions, environment — are important for understanding the complex role of mergers in galaxy evolution. For example, mergers between gas-poor, early-type galaxies in rich environments have been invoked to explain the stellar mass build-up of today's most massive ellipticals (e.g., van Dokkum 2005; Bell et al. 2007. Each of the approaches given above will yield independent estimates of the galaxy merger rate as a function of redshift, stellar mass, color, and environment. However, each technique probes different stages of the merger process, and is sensitive to different merger parameters (i.e., gas fraction, mass ratio). Therefore, the comparison of the large merger samples selected in different ways can constrain how the merger sequence and parameter spaces are populated.

Finally, the cadence of the LSST observations will open several exciting new avenues. It will be possible to identify optically variable AGN (§ 10.5) in mergers and constrain the SMBH growth as a function of merger stage, mass, and redshift. With millions of galaxy mergers with high star formation rates, we will detect a significant number of supernovae over the ten-year LSST survey. We will be able to determine the rate of SN I and II (Chapter 11) in mergers, and obtain independent constraints on the merger star formation rates and initial stellar mass functions.

9.10 Special Populations of Galaxies

There are a variety of approaches to classifying galaxies and searching for outliers. In broad terms, one attempts to define a manifold of galaxies through the multi-dimensional space of the measured

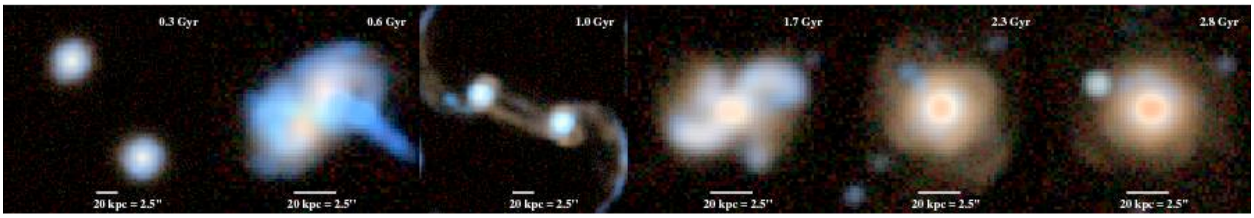

Figure 9.17: At full LSST depth, strong asymmetries, tidal tails, and post-merger fine structures will be observable for gas-rich major mergers at $z \gtrsim 1$. These images show the progression of a gas-rich equal mass disk merger, as it would appear at $z = 1$ in $r - i - z$ color. These are from a hydrodynamical simulation which includes gas, star formation, and dusty radiative transfer (Lotz et al. 2008b). During the initial encounter at $t = 0.6$ Gyr and the final merger at $t = 1.7$ Gyr, strong blue distortions are visible on scales of a few arc-seconds. After the first pass at $t = 1$ Gyr, tidal tails of $\sim 5 - 10''$ are detectable at $\mu_i < 27$ mag/arcsec^2. Faint shells, tidal features, and blue tidal dwarfs will be apparent at full LSST depth for up to a Gyr after the final merger ($t = 2.3 - 2.8$ Gyr), and are observed in deep HST and CFHTLS images.

parameters. Scientific discoveries come both from defining this manifold — which is equivalent to measuring galaxy scaling relations, their linearity, and their scatter — and trying to understand the outliers.

Approaches to defining the manifold include training sets and neural networks, principal component analysis, decision trees, self-organizing maps, and a variety of others. Training sets of millions of objects in each redshift interval will reveal subtle variations within known astrophysical phenomena. For example, for well-resolved galaxies at $z \lesssim 0.2$, LSST can characterize lopsidedness – as a function of color and environment – at a much higher S/N than any previous survey. Phenomena that were either overlooked or ascribed to cosmic variance in smaller samples will be revealed and quantified using the LSST images and database.

With millions of high S/N training examples to define the locus of "normal" galaxies, we can expect a wealth of scientific discoveries in the outlier population. The outlier population will include rare kinds of strong gravitational lenses (Chapter 12), which may have slipped through automated lens finders. It will include unusual galaxy interactions — e.g., ring galaxies, polar ring galaxies, or three and four-body interactions — follow-up studies of which may yield insights into the shapes of dark-matter halos (Iodice et al. 2003) or how star formation is triggered in merger events (di Matteo et al. 2008). It will include rare projections of galaxies that can be used to probe dust within spiral arms (Holwerda et al. 2007).

9.11 Public Involvement

We have already described in § 4.5 the very successful Galaxy Zoo project, whereby hundreds of thousands of citizen scientists have made a real contribution to scientific research by classifying the SDSS images of galaxies by eye. This motivates a new generation of "Zoos", and one that would provide equally remarkable science value will be Merger Zoo. In fact, the SDSS Galaxy Zoo team has specifically indicated that this is needed. Galaxy Zoo-Classic provides morphological classifications of spirals and ellipticals and "mergers." All oddball galaxies that cannot be placed into one of the other two classes are classified as mergers. When LSST generates deeper images of larger numbers of mergers, at increasing look-back times, then something must be done to classify these mergers (§ 9.9). Over the past three decades, collision/merger modelers have succeeded in deriving reasonable (unique?) models for of order 100–200 merging systems. This is a very small number. It is exceedingly hard because there are one to two dozen input parameters to even the simplest models, there are unknown viewing angles, and there is an unknown age for each system. It is virtually impossible to train a computer model to emulate the human pattern recognition capabilities that our eyes and our brains provide. This has been tried with genetic algorithms with limited success. Fortunately, as Galaxy Zoo has demonstrated, we can enlist the aid of hundreds of thousands of pairs of eyes to look at merger models, to compare with images, and to decide which model matches a given observation. Plans for Merger Zoo are now under way, involving the original Galaxy Zoo team, plus merger scientists at George Mason University and outreach specialists at Adler Planetarium and Johns Hopkins University. It will be deployed to work with SDSS mergers, so that Merger Zoo (or more likely, its descendant) will be ready for the flood of galaxy data from LSST in the future.

References

Abate, A., Wittman, D., Margoniner, V. E., Bridle, S. L., Gee, P., Tyson, J. A., & Dell'Antonio, I. P., 2009, *ApJ*, 702, 603

Abraham, R. G., van den Bergh, S., Glazebrook, K., Ellis, R. S., Santiago, B. X., Surma, P., & Griffiths, R. E., 1996, *ApJS*, 107, 1

Adelberger, K. L., Erb, D. K., Steidel, C. C., Reddy, N. A., Pettini, M., & Shapley, A. E., 2005a, *ApJL*, 620, L75

Adelberger, K. L., Steidel, C. C., Pettini, M., Shapley, A. E., Reddy, N. A., & Erb, D. K., 2005b, *ApJ*, 619, 697

Bahcall, N. A., Dong, F., Hao, L., Bode, P., Annis, J., Gunn, J. E., & Schneider, D. P., 2003, *ApJ*, 599, 814

Barrientos, L. F., Schade, D., López-Cruz, O., & Quintana, H., 2004, *ApJS*, 153, 397

Bell, E. F., McIntosh, D. H., Katz, N., & Weinberg, M. D., 2003, *ApJS*, 149, 289

Bell, E. F. et al., 2004, *ApJ*, 608, 752

Bell, E. F., Zheng, X. Z., Papovich, C., Borch, A., , & Meisenheimer, K., 2007, *ApJ*, 663, 834

Berlind, A. A., & Weinberg, D. H., 2002, *ApJ*, 575, 587

Bernstein, G. M., 1994, *ApJ*, 424, 569

Berrier, J. C., Bullock, J. S., Barton, E. J., Guenther, H. D., Zentner, A. R., & Wechsler, R. H., 2006, *ApJ*, 652, 56

Binney, J., 1977, *ApJ*, 215, 483

Blake, C., Collister, A., & Lahav, O., 2008, *MNRAS*, 385, 1257

Blakeslee, J. P. et al., 2003, *ApJL*, 596, L143

Blanton, M. R., & Berlind, A. A., 2007, *ApJ*, 664, 791

Blanton, M. R., Eisenstein, D., Hogg, D. W., Schlegel, D. J., & Brinkmann, J., 2005, *ApJ*, 629, 143

Blanton, M. R. et al., 2003, *ApJ*, 594, 186

Bouwens, R. J., Illingworth, G. D., Blakeslee, J. P., & Franx, M., 2006, *ApJ*, 653, 53

Bouwens, R. J., Illingworth, G. D., Franx, M., & Ford, H., 2008, *ApJ*, 686, 230

Bouwens, R. J. et al., 2004, *ApJL*, 606, L25

Bridge, C., & Carlberg, R., 2007, Bulletin of the American Astronomical Society, Vol. 38, The CFHTLS-Deep Catalog of Interacting Galaxies: Evolution of the Merger Fraction from $0.2 < z < 1.0$. p. 956

Bruzual, G., & Charlot, S., 2003, *MNRAS*, 344, 1000

Bullock, J. S., Wechsler, R. H., & Somerville, R. S., 2002, *MNRAS*, 329, 246

Bundy, K., Fukugita, M., Ellis, R. S., Kodama, T., & Conselice, C. J., 2004, *ApJL*, 601, L123

Bunker, A. J., Stanway, E. R., Ellis, R. S., & McMahon, R. G., 2004, *MNRAS*, 355, 374

Calzetti, D., Armus, L., Bohlin, R. C., Kinney, A. L., Koornneef, J., & Storchi-Bergmann, T., 2000, *ApJ*, 533, 682

Carlberg, R. G. et al., 2000, *ApJL*, 532, L1

Carlberg, R. G., Pritchet, C. J., & Infante, L., 1994, *ApJ*, 435, 540

Carlstrom, J. E. et al., 2009, ArXiv e-prints, 0907.4445

Coil, A. L. et al., 2006, *ApJ*, 638, 668

Coil, A. L., Hennawi, J. F., Newman, J. A., Cooper, M. C., & Davis, M., 2007, *ApJ*, 654, 115

Coil, A. L. et al., 2008, *ApJ*, 672, 153
Colín, P., Klypin, A. A., Kravtsov, A. V., & Khokhlov, A. M., 1999, *ApJ*, 523, 32
Conroy, C., & Wechsler, R. H., 2009, *ApJ*, 696, 620
Conroy, C., Wechsler, R. H., & Kravtsov, A. V., 2006, *ApJ*, 647, 201
Conselice, C. J., 2003, *ApJS*, 147, 1
Cooper, M. C. et al., 2006, *MNRAS*, 370, 198
Cooper, M. C., Newman, J. A., Madgwick, D. S., Gerke, B. F., Yan, R., & Davis, M., 2005, *ApJ*, 634, 833
Cooper, M. C., Tremonti, C. A., Newman, J. A., & Zabludoff, A. I., 2008, *MNRAS*, 390, 245
Cooray, A., 2006, *MNRAS*, 365, 842
Croton, D. J. et al., 2005, *MNRAS*, 356, 1155
—, 2006, *MNRAS*, 365, 11
Dalcanton, J. J., Spergel, D. N., Gunn, J. E., Schmidt, M., & Schneider, D. P., 1997, *AJ*, 114, 635
de Blok, W. J. G., & Bosma, A., 2002, *A&A*, 385, 816
Dekel, A. et al., 2009, *Nature*, 457, 451
Dekel, A., & Lahav, O., 1999, *ApJ*, 520, 24
di Matteo, P., Bournaud, F., Martig, M., Combes, F., Melchior, A.-L., & Semelin, B., 2008, *A&A*, 492, 31
Dickinson, M. et al., 2004, *ApJL*, 600, L99
Draine, B. T., & Lee, H. M., 1984, *ApJ*, 285, 89
Dressler, A., 1980, *ApJ*, 236, 351
Efstathiou, G., & Rees, M. J., 1988, *MNRAS*, 230, 5P
Faber, S. M. et al., 2007, *ApJ*, 665, 265
Fakhouri, O., & Ma, C.-P., 2008, *MNRAS*, 386, 577
Francke, H. et al., 2008, *ApJL*, 673, L13
Galaz, G., Cortés, P., Bronfman, L., & Rubio, M., 2008, *ApJL*, 677, L13
Galaz, G., Dalcanton, J. J., Infante, L., & Treister, E., 2002, *AJ*, 124, 1360
Galaz, G., Villalobos, A., Infante, L., & Donzelli, C., 2006, *AJ*, 131, 2035
Gardner, J. P. et al., 2006, *Space Science Reviews*, 123, 485
Giavalisco, M. et al., 2004, *ApJL*, 600, L93
Gonzalez, J. E., Lacey, C. G., Baugh, C. M., Frenk, C. S., & Benson, A. J., 2008, ArXiv e-prints, 0812.4399
Goto, T., Yagi, M., Tanaka, M., & Okamura, S., 2004, *MNRAS*, 348, 515
Gottlöber, S., Klypin, A., & Kravtsov, A. V., 2001, *ApJ*, 546, 223
Hansen, S. M., Sheldon, E. S., Wechsler, R. H., & Koester, B. P., 2009, *ApJ*, 699, 1333
Hogg, D. W. et al., 2003, *ApJL*, 585, L5
Holwerda, B. W., Keel, W. C., & Bolton, A., 2007, *AJ*, 134, 2385
Hopkins, P. F., Hernquist, L., Cox, T. J., & Kereš, D., 2008, *ApJS*, 175, 356
Impey, C., & Bothun, G., 1989, *ApJ*, 341, 89
Iodice, E., Arnaboldi, M., Bournaud, F., Combes, F., Sparke, L. S., van Driel, W., & Capaccioli, M., 2003, *ApJ*, 585, 730
Kauffmann, G. et al., 2003, *MNRAS*, 341, 33
Kereš, D., Katz, N., Fardal, M., Davé, R., & Weinberg, D. H., 2009, *MNRAS*, 395, 160
Kravtsov, A. V., Berlind, A. A., Wechsler, R. H., Klypin, A. A., Gottlöber, S., Allgood, B., & Primack, J. R., 2004, *ApJ*, 609, 35
Lacey, C., & Cole, S., 1993, *MNRAS*, 262, 627
Le Fèvre, O. et al., 2000, *MNRAS*, 311, 565
Lee, K.-S., Giavalisco, M., Gnedin, O. Y., Somerville, R. S., Ferguson, H. C., Dickinson, M., & Ouchi, M., 2006, *ApJ*, 642, 63
Li, Y. et al., 2007, *ApJ*, 665, 187
Limber, D. N., 1953, *ApJ*, 117, 134
Lin, L. et al., 2004, *ApJL*, 617, L9
Lotz, J. M. et al., 2008a, *ApJ*, 672, 177
Lotz, J. M., Jonsson, P., Cox, T. J., & Primack, J. R., 2008b, *MNRAS*, 391, 1137
Lotz, J. M., Primack, J., & Madau, P., 2004, *AJ*, 128, 163
Malhotra, S. et al., 2005, *ApJ*, 626, 666
Maraston, C., 2005, *MNRAS*, 362, 799
Martínez, V. J., & Saar, E., 2002, Statistics of the Galaxy Distribution. Published by Chapman & Hall/CRC, Boca Raton

Martínez-Delgado, D., Peñarrubia, J., Gabany, R. J., Trujillo, I., Majewski, S. R., & Pohlen, M., 2008, *ApJ*, 689, 184

Ménard, B., Kilbinger, M., & Scranton, R., 2009a, ArXiv e-prints, 0903.4199

Ménard, B., Scranton, R., Fukugita, M., & Richards, G., 2009b, ArXiv e-prints, 0902.4240

Mieske, S., Hilker, M., & Infante, L., 2003, *A&A*, 403, 43

Mihos, J. C., Harding, P., Feldmeier, J., & Morrison, H., 2005, *ApJL*, 631, L41

Oemler, A. J., 1974, *ApJ*, 194, 1

O'Neil, K., Hofner, P., & Schinnerer, E., 2000a, *ApJL*, 545, L99

O'Neil, K., Schinnerer, E., & Hofner, P., 2003, *ApJ*, 588, 230

O'Neil, K., Verheijen, M. A. W., & McGaugh, S. S., 2000b, *AJ*, 119, 2154

Ouchi, M. et al., 2004, *ApJ*, 611, 685

Padmanabhan, N., White, M., & Eisenstein, D. J., 2007, *MNRAS*, 376, 1702

Patton, D. R., Carlberg, R. G., Marzke, R. O., Pritchet, C. J., da Costa, L. N., & Pellegrini, P. S., 2000, *ApJ*, 536, 153

Patton, D. R. et al., 2002, *ApJ*, 565, 208

Peebles, P. J. E., 1980, The large-scale structure of the universe. Princeton University Press

Purcell, C. W., Bullock, J. S., & Zentner, A. R., 2007, *ApJ*, 666, 20

Reddy, N. A., & Steidel, C. C., 2009, *ApJ*, 692, 778

Reddy, N. A., Steidel, C. C., Pettini, M., Adelberger, K. L., Shapley, A. E., Erb, D. K., & Dickinson, M., 2008, *ApJS*, 175, 48

Rees, M. J., & Ostriker, J. P., 1977, *MNRAS*, 179, 541

Robertson, B., Li, Y., Cox, T. J., Hernquist, L., & Hopkins, P. F., 2007, *ApJ*, 667, 60

Schechter, P., 1976, *ApJ*, 203, 297

Shara, M. M., 2006, *AJ*, 131, 2980

Shen, Y. et al., 2007, *AJ*, 133, 2222

Sheth, R. K., Mo, H. J., & Tormen, G., 2001, *MNRAS*, 323, 1

Sheth, R. K., & Tormen, G., 1999, *MNRAS*, 308, 119

Silk, J., 1977, *ApJ*, 211, 638

Springel, V. et al., 2005, *Nature*, 435, 629

Stewart, K. R., Bullock, J. S., Barton, E. J., & Wechsler, R. H., 2009, *ApJ*, 702, 1005

Swanson, M. E. C., Tegmark, M., Blanton, M., & Zehavi, I., 2008, *MNRAS*, 385, 1635

Tinker, J., Kravtsov, A. V., Klypin, A., Abazajian, K., Warren, M., Yepes, G., Gottlöber, S., & Holz, D. E., 2008, *ApJ*, 688, 709

Vale, A., & Ostriker, J. P., 2006, *MNRAS*, 371, 1173

Vallenari, A., Schmidtobreick, L., & Bomans, D. J., 2005, *A&A*, 435, 821

van den Bosch, F. C., Yang, X., & Mo, H. J., 2003, *MNRAS*, 340, 771

van den Bosch, F. C. et al., 2007, *MNRAS*, 376, 841

van Dokkum, P. G., 2005, *AJ*, 130, 2647

Verde, L. et al., 2002, *MNRAS*, 335, 432

Wechsler, R. H., Bullock, J. S., Primack, J. R., Kravtsov, A. V., & Dekel, A., 2002, *ApJ*, 568, 52

White, S. D. M., & Rees, M. J., 1978, *MNRAS*, 183, 341

Woo, J., Courteau, S., & Dekel, A., 2008, *MNRAS*, 390, 1453

Yan, H., Dickinson, M., Giavalisco, M., Stern, D., Eisenhardt, P. R. M., & Ferguson, H. C., 2006, *ApJ*, 651, 24

Yan, H., & Windhorst, R. A., 2004, *ApJL*, 612, L93

Yang, X., Mo, H. J., & van den Bosch, F. C., 2008, *ApJ*, 676, 248

Zehavi, I. et al., 2004, *ApJ*, 608, 16

—, 2005, *ApJ*, 630, 1

Zepf, S. E., & Koo, D. C., 1989, *ApJ*, 337, 34

Zheng, Z. et al., 2005, *ApJ*, 633, 791

Zheng, Z., Coil, A. L., & Zehavi, I., 2007, *ApJ*, 667, 760

Zhong, G. H., Liang, Y. C., Liu, F. S., Hammer, F., Hu, J. Y., Chen, X. Y., Deng, L. C., & Zhang, B., 2008, *MNRAS*, 391, 986